Master's thesis

NTNU
Norwegian University of Science and Technology
Faculty of Natural Sciences
Department of Chemical Engineering

Tanja Bunevska

Characterization of a solvent for chemical absorption-based CO2 capture

Master's thesis in Chemical Engineering
Supervisor: Professor Hanna Knuutila
Co-supervisor: Researcher Ardi Hartono
July 2021

NTNU
Norwegian University of Science and Technology

Tanja Bunevska

Characterization of a solvent for chemical absorption-based CO2 capture

Master's thesis in Chemical Engineering
Supervisor: Professor Hanna Knuutila
Co-supervisor: Researcher Ardi Hartono
July 2021

Norwegian University of Science and Technology
Faculty of Natural Sciences
Department of Chemical Engineering

NTNU
Norwegian University of
Science and Technology

Abstract

The diploma thesis is focused on the thermodynamic characterization of an aqueous 3-amino-1-propanol (AP) solution, which is used as a promising solvent for post-combustion CO_2 capture from exhaust gases. The theoretical part contains a description of the solvent properties and the thermodynamic model selected for representation of the CO_2 behavior in the solvent blend. The main task of this work was divided in two optimization sections. The first section was devoted to modeling of the vapor–liquid equilibrium (VLE) of the binary AP-water system using the NRTL activity coefficient framework. In the second section, the model was extended by the electrolyte NRTL framework including CO_2 for a complete description of phase equilibrium in the ternary AP-H_2O-CO_2 system. Model elaboration and calculations were done in the MATLAB programming language. A literature review of all available VLE data was performed and the collected data were used to regress the interaction parameters of the NRTL model. For the full description of the ternary system, the phase equilibrium was coupled with the chemical reactions in the liquid phase.

Representation of the simulation results showed a very good agreement with the experimental data and a reasonable description of the CO_2 solubility in the selected alkanolamine solution. The developed model was further used to describe the liquid phase speciation and heat of absorption evaluation that is directly related to the energy requirements of the chemical absorption process. Regressed interaction parameters and chemical equilibrium constants in this work can be used in the design and simulation of the process.

Acknowledgement

This project was done at the Norwegian University of Science and Technology to accomplish the course TKP4900 - "Chemical Process Technology, Master's Thesis". It was written during the spring semester of the academic year of 2020/2021 at the Department of Chemical Engineering.

This way, I would like to thank everyone supporting me in any kind of way during the journey of working on this thesis project.

First of all, I would like to thank my supervisor, Professor Hanna Knuutila, for giving me the opportunity to join the CO_2 team. Also, I am grateful for her kindness, support, expertise and advice during our time working together. I am delighted that I got the opportunity of enriching my knowledge in the topic of absorption activities, and to have weekly meetings related to the topic. It was a great experience I feel like it will help me in the future as well. It was an honor to work with her.

I would like to express my gratitude to my co-supervisor Dr. Ardi Hartono for his patience, help and his time, since he was always ready to discuss my questions and concerns related to the project.

Last but not least, I would like to thank my family and friends for the constant support.

Table of Contents

List of Figures ix
List of Tables x
List of Abbreviations xi
1 Introduction 13
2 Theoretical part 14
2.1 Motivation 14
2.2 Carbon capture technology 15
2.3 Separation methods for CO_2 capture 16
2.4 Characterization of solvents 17
2.4.1 Loading 17
2.4.2 Cyclic capacity 17
2.4.3 Heat of absorption 18
2.5 Alkanolamines 18
2.6 Basic chemistry and kinetics of amines 19
2.7 3-Amino-1-propanol 20
2.8 Reactions occuring in aqueous AP solution in the presence of CO_2 20
2.9 Phase equilibrium 21
2.10 Activity coefficient 21
2.10.1 NRTL equation 21
2.10.2 e-NRTL equation 22
2.10.2.1 Long-range contribution 23
2.10.2.2 Born correction 23
2.10.2.3 Short-range contribution 23
2.11 Test of thermodynamic consistency 24
3 Aim of the work 26
4 Work methodology 27
4.1 Binary system equilibrium description methodology 27
4.2 Ternary system equilibrium description methodology 30
5 Results and discussion 35
5.1 Results of binary phase equilibrium data simulation 35
5.1.1 Accuracy of the model 38
5.2 Full model prediction of the ternary AP-H_2O-CO_2 system 40
5.2.1 Accuracy of the model 44
5.3 Speciation 45
5.4 Heat of absorption 46

5.5 Discussion 48
6 Conclusion 49
References 50
Appendix 1 54

List of Figures

Figure 2.1: Evolution of temperature, sea level, GHGs concentrations and anthropogenic CO_2 emissions [5] 14
Figure 2.2: Warming versus cumulative CO2 emissions [5] 15
Figure 2.3: Technology options for CO_2 separation [10] 17
Figure 2.4: Example of primary alkanolamine (Monoethanolamine) 19
Figure 2.5: Example of secondary alkanolamine (Diethanolamine) 19
Figure 2.6: Example of tertiary alkanolamine (Triethanolamine) 19
Figure 2.7: Example of sterically hindered alkanolamine (2-piperidine ethanol) 19
Figure 2.8: Structural formula of 3-amino-1-propanol 20
Figure 2.9: Illustration of thermodynamic consistency test 25
Figure 4.1: Optimization algorithm for the model parameters 29
Figure 4.2: Optimization algorithm for the ternary AP-H_2O-CO_2 system 32
Figure 4.3: Optimization procedure using the PSO algorithm [54] 33
Figure 5.1: Isothermal Pxy diagram for binary AP - water system at: a) 373 K, b) 353 K, c) 368 K, d) 358 K (Points [37]) 35
Figure 5.2: Activity coefficients of AP at: a) 373 K, b) 353 K, c) 368 K, d) 358 K. 36
Figure 5.3: Isobaric Txy data for binary AP-water system at: 533 mbar (blue color), 667 mbar (red color), 800 mbar (green color); 37
Figure 5.4: Excess enthalpy dependence of the AP-water mixture composition at: 298 K (black color), 313 K (blue color), 323 K (red color); 37
Figure 5.5: Excess heat capacity dependence of the AP-water mixture composition at: 303 K (black color), 308 K (red color), 313 K (blue color), 323 K (green color); 37
Figure 5.6: Test of thermodynamic consistency for binary AP-water system at: a) isothermal condition, b) isobaric condition 38
Figure 5.7: Parity plot between model representation and experimental total pressure data; 39
Figure 5.8: Parity plot between model representation and experimental excess enthalpy data 39
Figure 5.9: Parity plot between model representation and experimental points of bubble temperature data 39
Figure 5.10: CO_2 partial pressure dependence as a function of loading at: 293 K, 313 K, 333 K, 353 K, 373 K and [AP] = 7 M; 41
Figure 5.11: CO_2 partial pressure dependence as a function of loading at 313 K and [AP] = 3.9 M (black color), [AP] = 5 M (blue color) 42
Figure 5.12: CO_2 partial pressure dependence as a function of loading at: 298 K, 313 K, 323 K, 333 K, 343 K, 373 K, 393 K and [AP] = 2 M 43
Figure 5.13: CO_2 partial pressure dependence as a function of loading at: 298 K, 313 K, 323 K, 333 K and [AP] = 1.3 M 43
Figure 5.14: CO_2 partial pressure dependence as a function of loading at: 313 K, 343 K, 373 K, 393 K; a) [AP] = 5 M; b) [AP] = 4 M 44
Figure 5.15: Parity plot between experimental and model represented CO_2 partial pressure 44
Figure 5.16: Model representation of the speciation in 15 mass % of AP 45
Figure 5.17: eNRTL model representation of the heat of absorption as a function of loading at 313 K and 15 mass % of AP ([AP] = 2 M) 46
Figure 5.18: eNRTL model representation of the heat of absorption as a function of loading at 313 K and 30 mass % of MEA 47

List of Tables

Table 2.1: Summarization of advantages and disadvantages of CO2 capture technologies [6].....16
Table 4.1: Summarization of all available data used in model parameters fitting 28
Table 4.2: Summary of all available data used in the model parameters fitting.....30
Table 4.3: Pure component properties [47].....30
Table 4.4: Antoine equation coefficients of molecular species; [a] - taken from Aspen Plus database [47]; [b] - taken from DECHEMA database [37]; 31
Table 4.5: Dielectric constants of pure components [48] 31
Table 4.6: Correlations used in the ternary eNRTL model [47].....31
Table 4.7: Chemical equilibrium constants.....31
Table 4.8: PSO parameters [52].....34
Table 5.1: Calculated area tests of thermodynamic consistency for isobaric (D) and isothermal data (D-J); [a] - Points from in-house VLE data; [b] - Points from DECHEMA database [37];.....38
Table 5.2: Regressed binary interaction NRTL parameters 38
Table 5.3: Regressed eNRTL parameters; [a] - taken from Aspen Plus database [47].....40

List of Abbreviations

a	Activity	
A, B, C, D	Parameters	
cp	Heat capacity	[kJ/K]
d	Solvent density	[g/cm^3]
e	Electron charge	
G	Gibbs free energy	[kJ]
g	Parameter of the NRTL model	
H	Henry's constant	[kPa m^3/mol]
H	Enthalpy	[kJ/mol]
k	Boltzmann constant	
K	Equilibrium constant	
M	Molarity	[mol/dm^3]
M_i	Molecular mass of the i-th component	[g/mol]
N_0	Avogadro's number	
P	Pressure	[Pa]
P_i	Partial pressure of the i-th component	[Pa]
$P_i°$	Saturated vapor pressure of the i-th component	[Pa]
r	Born radius	[m]
R	Universal gas constant	[J/mol.K]
t	Temperature	[°C]
T	Thermodynamic temperature	[K]
v	Molar volume	[dm^3/mol]
x_i	Mole fraction of the i-th component in the liquid phase	
y_i	Mole fraction of the i-th component in the vapor phase	

Greek Letters

α	Liquid phase loading of CO_2 [mol CO_2 / mol amine]	
α	NRTL non-randomness factor	
γ	Activity coefficient	
ε	Dielectric constant	
ξ	Extent of reaction	
μ	Chemical potential	
υ	Stochiometry coefficient	
ρ	Closest approach parameter of the Pitzer-Debye-Huckel equation	
τ	NRTL interaction parameter	
Φ_1, Φ_2	Acceleration coefficients	
ω	Acentric factor	
$\emptyset_i$	Fugacity coefficient	

Subscript

abs	Absorption
a, a', a''	Anion
c, c', c''	Cation

c	Critical property
i, j, k	Denotation of components
g	Vapor phase
m, m’	Molecular species
s	Solvent
Superscript	
E	Excess function
lc	Local composition
*	Pure component
°	Standard state
Acronyms	
AP	3-amino-1-propanol
AARD	Average absolute relative deviation
CCS	Carbon capture and storage
CO_2	Carbon dioxide
EOR	Enhanced Oil Recovery
eNRTL	(Electrolyte Non-Random Two liquid) model
MEA	Monoethanolamine
NRTL	(Non-Random Two liquid) model
NTNU	Norwegian University of Science and Technology
PSO	Particle swarm optimization
VLE	Vapor Liquid Equilibrium

1 Introduction

One of the key problems of our industrialized civilization and social economic system is the destabilization of the biosphere by manmade emissions, which can no more be controlled and absorbed by the natural processes [1]. Due to the population growth, global energy demand is increasing rapidly. Fossil fuel combustion supplies more than 85% of the energy for industrial activities and is the main source of the greenhouse gases (GHG) in the form of CO_2 [2]. CO_2 has not only a negative impact on the environment, but also at higher concentration is directly "lethal" for the human body [1]. Even today renewable energy is of a very big interest, it could not completely replace fossil fuels in the near future. "Today, nearly every service people use and every product consumers buy has a fossil fuel somewhere in how it is made or delivered" (Shell). Fossil fuels are inevitable in our lives and the goal is to limit the global temperature increase to 2°C above pre-industrial levels by 2100 [3].

Carbon Capture and Storage (CCS) is an exciting area of research and development for today's scientists. This method is extracting CO_2 from gas streams, whether power production or industrial origin and storing it in large quantities in subsurface geological formations. On this way, application of CCS is expected to play an important role in the fight against climate change and deliver half of the global emissions reduction by 2050 [4]. But building up a business model of a new technology, such as CCS, needs to prove not only its economic viability at a reasonable carbon avoided cost, but also its ability to be implemented on a large scale. This technology is highly costly because exhibits a large technological diversity in each of its three steps (capture, transport, storage), where capture cost represents 85% of the CCS final cost. For this reason, improvements in the CO_2 capture technology are of the biggest importance.

In the heart of every design and simulation process lies an accurate thermodynamic model that should take into account the deviations from the ideal behavior in a mixture of chemical substances. This work was devoted to a chemical absorption as the most mature technology for post-combustion CO_2 capture. A thermodynamic model has been developed that will provide a description of both phase and chemical equilibrium in the liquid phase. For this purpose, CO_2 solubility into an aqueous alkanolamine solution of 3-amino-1-propanol was investigated.

2 Theoretical part

2.1 Motivation

Human activities have important influence on the climate system, and they are responsible for a phenomenon called global warming, that can cause irreversible risks for people and ecosystems. Observed changes in the climate system such as: ocean acidification, sea level rise, changes in extreme weather and climate event and many others are just indication that people have to take actions and save our planet (Figure 2.1) [5].

Since the industrial era, the pH of the ocean surface water has decreased by 0.1 with taking CO_2 from the atmosphere which results by 26% higher ocean acidity. Over the period 1992 to 2011 the Greenland and Antarctic ice sheets have been losing mass due to the increased surface temperature. From the mid-19th century global sea level has risen by 0.19 m [5].

This is all driven by the economic and population growth followed by increased anthropogenic greenhouse gas emissions in the atmosphere. Since the pre-industrial era gases like carbon dioxide, methane and nitrous oxide have a dominant effect on the Earth's warming. Figure 2.2 shows how the surface temperature will increase in the future if we do not take now any actions.

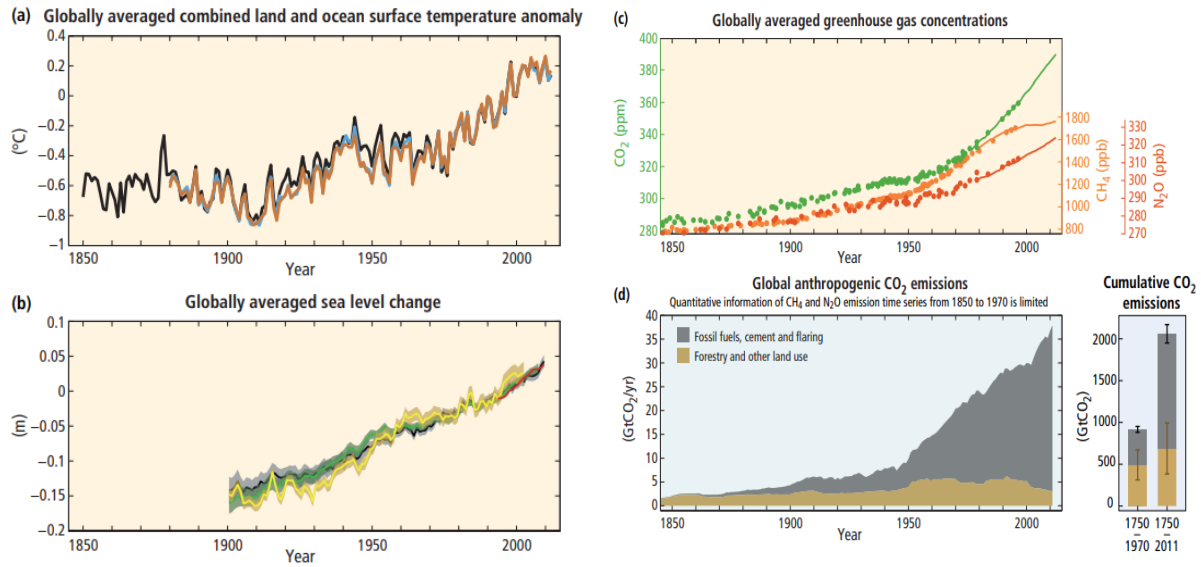

Figure 2.1 Evolution of temperature, sea level, GHGs concentrations and anthropogenic CO_2 emissions [5]

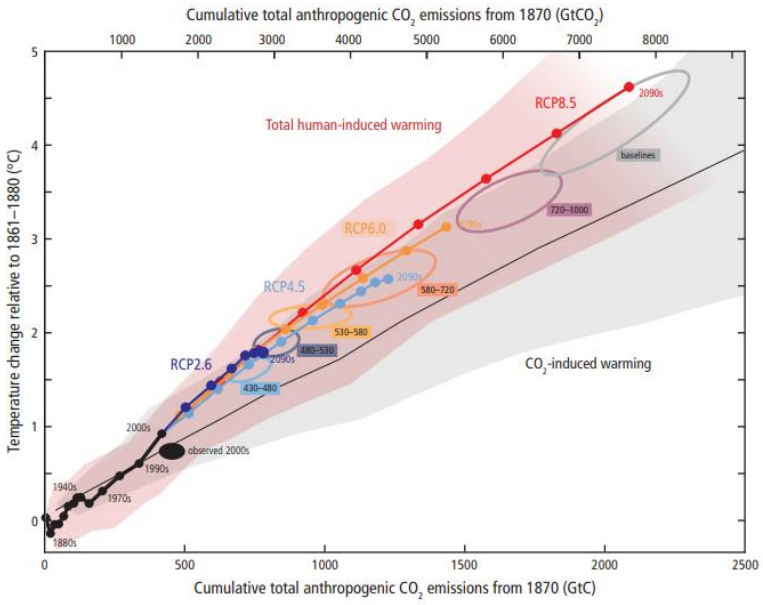

Figure 2.2 Warming versus cumulative CO2 emissions [5]

2.2 Carbon capture technology

The purpose of Capture and Storage of Carbon Dioxide (CCS) is to reduce carbon dioxide emissions to the atmosphere. CCS consist of several steps: CO_2 removal from flue gases produced by combustion of fossil fuels in power plants and industrial sectors for energy production, compression and liquefaction of the CO_2 so that it can be transported and storage of the CO_2 in aquifers and empty gas fields.

Today only 17 large-scale CCS projects are currently operational and their main usage for the separated CO_2 is in Enhanced Oil Recovery [EOR] [7] from the reservoir for dissolving CO_2 in the oil, thus decreasing the oil viscosity and increasing its flow. Four main pathways to CCS can be classified as follows [8]:

- Post-combustion

  Carbon dioxide is removed from the flue gas produced by the combustion of the fossil fuels in the air. In general, chemical solvent is used to capture the small fractions of CO_2 present in the flue gas and is recovered by heating, while the CO_2 is compressed, transported and stored.
- Pre-combustion

  In the pre-combustion technology, carbon dioxide is removed before combustion takes place. Fuel is processed by gasification or steam methane reforming and a syngas rich of carbon monoxide and hydrogen is produced. Additional hydrogen, together with the carbon dioxide is produced by reacting the carbon monoxide with steam in a catalytic reactor called shift reactor. The final process provides CO_2 separation and production of clean burning hydrogen.
- Oxyfuel combustion

  In oxyfuel combustion fuel is combusted in pure oxygen instead of air. The produced flue gas contains of water vapor and high CO_2 concentrations. CO_2 can be easily separated because the capture process consists mainly of water condensation.

- Industrial separation

  The CO_2 removal from the large-scale industrial processes is widely used today. The pre-combustion technology is commonly used in the hydrogen production industry, while the post-combustion technique is employed for separation of the CO_2 from natural gas.

At this point, post-combustion capture system is the only proven technology compatible with the world's huge investment in the fossil fuel infrastructure. Its advantage is that if the capture system encounters difficulty, the power plant can continue to operate while the CO_2 is vented to atmosphere, which is not possible in case with pre-combustion system. The advantages and disadvantages of these capture technologies are presented in Table 2.1.

Table 2.1 Summarization of advantages and disadvantages of CO2 capture technologies [6]

Capture technology	Advantages	Disadvantages
Post-combustion	Existing technology	Energy penalty due to solvent regeneration
	Retrofit to existing power plant designs	Loss of solvent
	Extra removal of NO_x and SO_x	
Pre-combustion	Existing technology	Combustion of hydrogen is a challenge
	Very low emissions	Cooling of gas to capture CO_2 is necessary
		Efficiency loss in water-gas shift section
Oxyfuel combustion	Existing technology	High energy input for air separation
	Absence of nitrogen → no NO_x emissions	Combustion in pure oxygen is complicated
	Absence of nitrogen → low volume of gases and reduction of the entire process size	

2.3 Separation methods for CO_2 capture

Separation methods for CO_2 capture from flue gases can be divided as follows (see Figure 2.3):

- Chemical and Physical absorption. Monoethanolamine (MEA) is the most extensively employed solvent in the absorption-desorption technology.
- Physical adsorption
- Membrane technologies
- Cryogenic separation

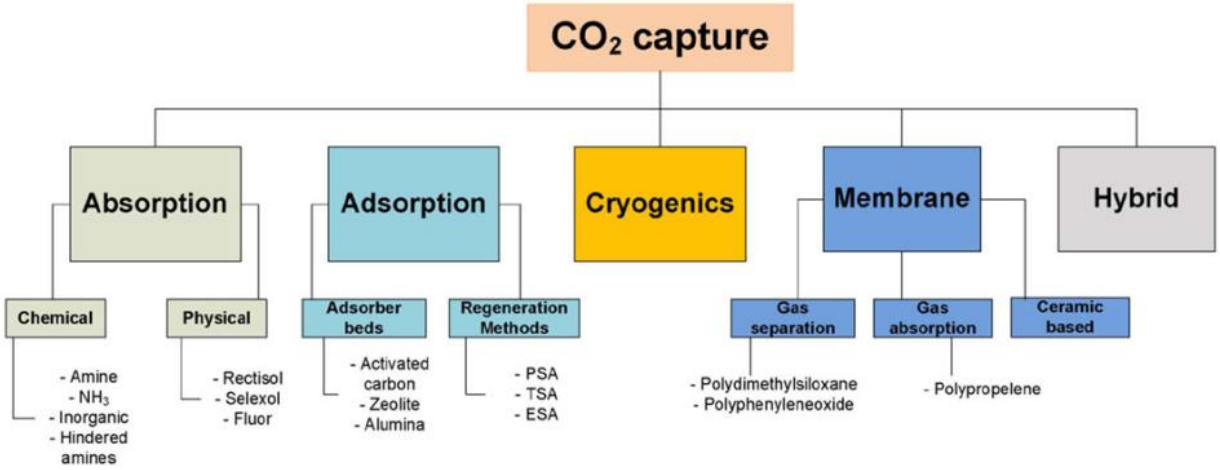

Figure 2.3 Technology options for CO_2 separation [10]

CO_2 removal by absorption and stripping with aqueous alkanolamine is a well-understood and currently the only commercial technology for post-combustion capture of CO_2. Alakolamine scrubbing is widely used technology for flue gas desulfurization in refinery since 1936 [11]. Because of the high costs and energy requirements, improvements in alkanolamine-based absorption technologies are of interest with the aim to reduce both capital and operation costs.

2.4 Characterization of solvents

As mentioned before, absorption-desorption is an energy demanding technology, where the highest costs are connected with the energy required in the desorption process. In the case of chemical absorption, solvent absorbs and reacts with the CO_2, where the process is favored at low temperatures and high pressure. For shifting the absorption reaction and releasing the captured CO_2 from the solvent, high temperatures and low pressure are required. Understanding the absorption-reaction mechanism of CO_2 capture is necessary so that further improvements can be done for reducing the overall process costs. Since aqueous alkanolamine-based solvents are the most promising for post-combustion CO_2 capture several properties will be followed.

2.4.1 Loading

Loading *a* represents one of the most important solvent parameters which describes the amount of CO_2 absorbed by unit amount of solvent. It can be calculated by the equation [12]:

$$\alpha = \frac{mol\ CO_2 absorbed}{mol\ amine} \tag{2.1}$$

High absorption capacity means lower solvent circulation rates and equipment size which, in other words, means lower operation and investment costs.

2.4.2 Cyclic capacity

Another parameters that can contribute to lower regeneration energy consumption is a cyclic capacity. It is defined as difference in the CO_2 loading of the absorbent at absorption conditions (rich solution) and desorption conditions (lean solution), and is defined by the equation:

$$\Delta\alpha = \alpha_{reach} - \alpha_{lean} \tag{2.2}$$

Solvent with high cyclic capacity would be an advantage as it reduces the sensible heat loss and results in a smaller circulation flow rate [13]. Cyclic capacity is increasing with the concentration of the solvent. However, it should be mentioned that the higher the concentration of alkanolamine, the higher the viscosity of the solvents and their corrosivity. For example, the most common industrially used alkanolamine, MEA or monoethanolamine, represents 30% aqueous solution. At higher MEA concentration the solution is extremely corrosive. On the other hand, having a higher solvent concentration is desirable since the concentration and partial pressure of CO_2 in exhaust gases are very low.

2.4.3 Heat of absorption

Heat of absorption of CO_2 [kJ/mol] is defined as the heat released/needed during absorption of 1 mol of CO_2 in the solution. Having a low heat of absorption is desirable because it directly reduces the energy required in the recovery process. Absorption heat defined by the equation [12]:

$$H_{abs} = \sum_i \xi_i \Delta H_i \tag{2.3}$$

Where ξ_i is the extent of reaction [mol] and ΔH_i is the heat of reaction, or enthalpy of reaction "*i*" [kJ/mol].

The most desirable solvent for post-combustion CO_2 capturing will be the one which is environmentally friendly, resistant to degradation, non-toxic, non-corrosive, has low viscosity, offers fast reaction kinetics towards CO_2 sequestration and, preferably, is non-expensive [14].

For significant reduction of CO_2 capture process operation costs, thermal stability and resistance to oxidative degradation of the chosen solvent are very important. In flue gases, except carbon dioxide, can be present large number of other impurities such as: H_2S, NO_x, SO_x, O_2, as well as fly ash and, sometimes, mercury. These impurities can cause increased solvent loss, solvent contamination, foaming in the absorber and desorber, equipment fouling, erosion etc. The solvent must not only be active at low CO_2 partial pressure, but also it has to tolerate the presence of the above mentioned impurities.

2.5 Alkanolamines

The most promising solvents for post-combustion capturing of CO_2 with chemical absorption are alkanolamines. Alkanolamines have favorable chemical and physical properties since they contain hydroxyl and amino groups. Hydrogen bonds formed between the hydroxyl groups are responsible for the solvent vapor pressure and they increase alkanolamine solubility in water. On the other hand, CO_2 has acid properties and amino group is providing the necessary basicity so that the absorption can occur [15]. These solvents have also very high affinity for CO_2. This is very important as it make the technology highly selective towards CO_2.

Alkanolamine represent derivatives of ammonia. Based on the number of carbon atoms attached to the nitrogen, they are characterized as: primary (one hydrogen atom replaced with carbon atom), secondary (two hydrogen atoms replaced with two carbon atoms) and tertiary (three carbon atoms connected to the nitrogen) [16]. Sterically hindred alkanolamines represent primary alkanolamines, in which amino group is attached to a tertiary carbon atom or a secondary amine in which the amino group is

attached to a secondary or tertiary carbon atom [14]. Structural formulas of all these amine representatives are shown in Figure 2.4-2.7.

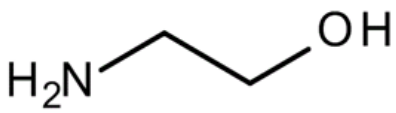

Figure 2.4 Example of primary alkanolamine (Monoethanolamine)

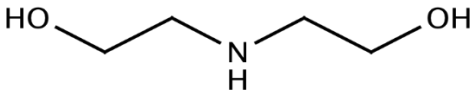

Figure 2.5 Example of secondary alkanolamine (Diethanolamine)

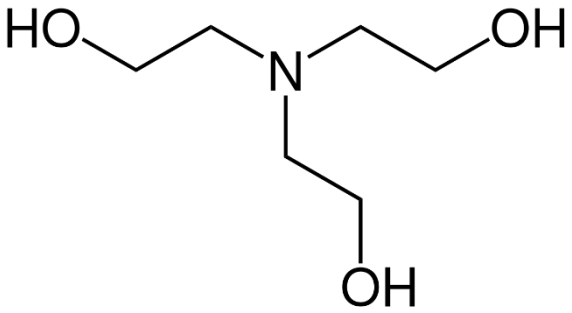

Figure 2.6 Example of tertiary alkanolamine (Triethanolamine)

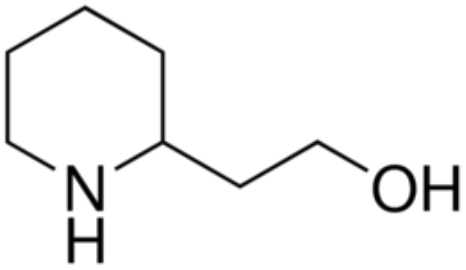

Figure 2.7 Example of sterically hindered alkanolamine (2-piperidine ethanol)

2.6 Basic chemistry and kinetics of amines

In the reaction of primary and secondary alkanolamines with CO_2, carbamates are formed. The reaction can be described by the equation [17]:

$$CO_2 + 2RNH_2 = RNHCOO^- + RNH_3^+ \quad (2.5)$$

These alkanolamines offer high absorption rate with CO_2 and high energy of regeneration because of the formation of carbamates connected with high heat of absorption. According to the stoichiometry, they are also characterized with lower absorption capacity since two alkanolamine molecules react with one CO_2 molecule with the maximum loading of 0.5 mol CO_2/mol amine.

Tertiary alkanolamines are slightly more basic than the other alkanolamines and in a reaction with CO_2 bicarbonate is formed. The reaction can be described by the equation [17]:

$$CO_2 + R_1R_2R_3N + H_2O = R_1R_2R_3NH^+ + HCO_3^- \quad (2.6)$$

For tertiary alkanolamines, low absorption rate of CO_2 and lower energy of regeneration are typical because of the formation of bicarbonate associated with low heat of absorption. Since one alkanolamine molecule is reacting with one CO_2 molecule, tertiary alkanolmines can achieve a theoretical loading of 1 mol CO_2/mol amine.

MEA or monoethanolamine is the most common alkanolamine-based solvent for CO_2 sequestration, primarily because of its high reactivity with CO_2 and low production cost. Although MEA-based scrubbing technology is suitable for post-combustion CO_2 capture from fossil-fired plants flue gas, it suffers from several issues, including high enthalpy of reaction, low absorption capacity, oxidative and thermal degradation, and equipment corrosion [14]. Capital and energy cost reduction of this process could be reached by using amine other than MEA [11].

2.7 3-Amino-1-propanol

3-Amino-1-propanol or AP is a linear primary alkanolamine with an amine-like odor. It is a colorless liquid at room temperature [18]. It is suitable for absorption of carbon dioxide with low concentrations in the gas streams [19] and is soluble with water, acetone, glycol, glycerol and glycol ethers [18]. This alkanolamine is of a very big interest. Mainly because alkanolamines with three carbon atoms have better CO_2 absorption capacity than others primary alkanolamines. On the other hand, it was found that further increase in carbon chain length between amino and hydroxyl groups, absorption rate of alkanolamines is decreasing [20]. AP has variety of applications, such as: an intermediate in the production of pharmaceuticals, cosmetics, corrosion inhibitors, synthetic resins and plasticizers [21]. Structural formula of AP is shown in the Figure 2.8.

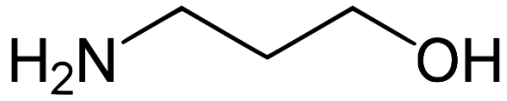

Figure 2.8 Structural formula of 3-amino-1-propanol

2.8 Reactions occuring in aqueous AP solution in the presence of CO_2

The process of absorption of acid gases can be described by two steps. As a first step, gas phase species must to be dissolved into the aqueous phase:

$$CO_{2\,(g)} \leftrightarrow CO_{2\,(aq)} \tag{2.7}$$

In the second step, the aqueous gas species are converted into ions through chemical reaction. The chemical reaction of CO_2 with 3-amino-1-propanol in aqueous solution takes place in the liquid phase and can be described by a complex mechanism, which includes several steps [21]:

- protonation of amine:

$$AP + H_2O \leftrightarrow APH^+ + OH^- \tag{2.8}$$

- carbamate formation:

$$AP + CO_2 + H_2O \leftrightarrow APCOO^- + H_3O^+ \tag{2.9}$$

- hydrolysis of carbon dioxide:

$$2H_2O + CO_2 \leftrightarrow H_3O^+ + HCO_3^- \tag{2.10}$$

- dissociation of water:

$$2H_2O \leftrightarrow H_3O^+ + OH^- \tag{2.11}$$

- dissociation of bicarbonate ion:

$$HCO_3^- + H_2O \leftrightarrow H_3O^+ + CO_3^{2-} \tag{2.12}$$

Traditionally, the chemical equilibrium can be defined by the equilibrium constant K [22]:

$$K = \prod_{i=1}^{n} a_i^{v_i} = \prod_{i=1}^{n} \gamma_i^{v_i} x_i^{v_i} \tag{2.13}$$

Where a_i is activity of component *i*, v_i is stoichiometric coefficient of component *i*, γ_i is activity coefficient and x_i is component i mole fraction in the liquid phase.

2.9 Phase equilibrium

Phase equilibrium governs the distribution of molecular species between the vapor and liquid phase and it can be described by the Gibbs formulation. He stated that at equilibrium, the chemical potential of species at a given temperature and pressure must to be same in both phases:

$$\mu_i^{vap}(T,P,n) = \mu_i^{liq}(T,P,n) \tag{2.14}$$

Compounds which are liquids at standard conditions, such as water and alkanolamines, have pure component reference state. In the case of an activity model for liquid phase and equation of state for the vapor phase, phase equilibrium for this non-supercritical components can be described as follows:

$$\emptyset_i y_i P = \gamma_i x_i P_i^{\circ} exp\left[\frac{v_i\left(P - P_i^{\circ}\right)}{RT}\right] \tag{2.15}$$

Where $\emptyset_i$ and γ_i are fugacity and activity coefficient of species *i*, respectively. The last term of equation (1.15) is called Poynting factor and at relatively low pressures is closed to unity.

Supercritical components, such as CO_2 which have gas-liquid properties above the critical temperature and pressure, will not exist as pure species in alkanolamine gas-treating system. Therefore they require a different reference state. The infinite dilution reference state can be used for these components and the following equation applies:

$$\emptyset_i y_i P = \gamma_i^* x_i H_i^{\propto} exp\left[\frac{v_i^{\propto}\left(P - P_i^{\circ}\right)}{RT}\right] \tag{2.16}$$

Where γ_i^* is activity coefficient of species *i* at infinite dilution, $H_i^{\propto}$ is Henry's constant for molecular solute *i* in pure water at the system temperature and at the vapor pressure of water.

More about phase equilibrium can be found at various thermodynamics textbooks [23-25].

2.10 Activity coefficient

An activity coefficient is a factor used in thermodynamics to account for deviations from ideal behaviour in a mixture of chemical substances [26]. There are several activity coefficient models that describe variation of the activity coefficient of a component with the liquid mixture composition. Among the most commonly used is the NRTL, which can be applied to polar mixtures. Other models include: Wilson, UNIQUAC, Van Laar, UNIFAC, Electrolyte NRTL. In these models, the activity coefficient approach is used to calculate the liquid mixture composition, while the vapor phase properties are calculated using an equation of state [26].

2.10.1 NRTL equation

Explaining the dependence of activity coefficients from composition using the NRTL equation (non-random two liquids) is particularly useful for the calculation of phase equilibria of multi-component systems or systems composed of components with limited miscibility. The NRTL model was proposed by Renon and Prausnitz and it is based on the Wilson's local composition concept and Scott's two liquid model theory [27]. For the *n*-component system for the excess Gibbs energy applies [28]:

$$\frac{G^E}{RT} = \sum_k^n \left(x_k \frac{\sum_j^n x_j \tau_{jk} G_{jk}}{\sum_j^n x_j G_{jk}} \right) \tag{2.17}$$

Activity coefficient of the *i*-th component in multi-component system is expressed [28]:

$$ln\,\gamma_i = \frac{\sum_j^n x_j \tau_{ji} G_{ji}}{\sum_j^n x_j G_{ji}} + \sum_k^n \frac{x_k G_{ik}}{\sum_j^n x_j G_{jk}} \left(\tau_{ik} - \frac{\sum_j^n x_j \tau_{jk} G_{jk}}{\sum_j^n x_j G_{jk}} \right) \tag{2.18}$$

$$G_{ij} = exp\left(-\alpha_{ij}\tau_{ij}\right) \tag{2.19}$$

$$\tau_{ji} = \frac{\left(g_{ji} - g_{ii}\right)}{RT} = \frac{\Delta g_{ji}}{RT} \tag{2.20}$$

$$G_{ji} = exp\left(-\alpha_{ji}\tau_{ji}\right) \tag{2.21}$$

$$\alpha_{ij} = \alpha_{ji} \qquad \tau_{ij} \neq \tau_{ji} \qquad \tau_{ii} = \tau_{jj} = 0 \tag{2.22}$$

The NRTL equation contains binary dimensionless parameters τ_{ij}, τ_{ij}, α_{ij} and α_{ji}. The parameter α_{ij} is related to the non-ideal behavior of mixing. Typically, the following applies: $\alpha_{ij} = \alpha_{ji}$. Parameter τ_{ij} is a function of the change of potential energies between the molecules *i* and *j* and between the molecules of the same component *j* [28].

The excess enthalpy, which indicates the temperature dependence of the Gibbs energy, can be determined by the Gibbs-Helmholtz equation [29]:

$$\left(\frac{\partial \left(\frac{G^E}{RT} \right)}{\partial (1/T)} \right)_{P,x} = -\frac{H^E}{R} \tag{2.23}$$

Another important thermodynamic property is excess the heat capacity which represents a second derivative of Gibbs energy with the respect to temperature [30]:

$$c_p^E = \left(\frac{\partial H^E}{\partial T} \right)_{P,x} \tag{2.24}$$

Since excess enthalpy and heat capacity are directly related to the temperature dependence of the activity coefficients, they significantly improve the modeling of temperature-dependent variables.

2.10.2 e-NRTL equation

The electrolyte non-random two liquid (e-NRTL) model was developed in the early 1980s by Chen and co-workers [31]. By using binary parameters, this model was generalized to represent the excess Gibbs energy and activity coefficients of aqueous multicomponent electrolyte systems and their deviation from ideality. The model considers two basic assumption: the local electroneutrality and ion-like repulsion assumption [32]. The like-ion repulsion assumption is based on the fact that repulsive forces between ions of the same charge are extremely large. Assuming this, the likelihood of finding ions of same charge in the near vicinity is very low. In addition, local electroneutrality must be satisfied. This means that distribution of ions around a central molecular species is so that the local ionic charge is zero.

Chen further proposed the excess Gibbs energy formulation to be a sum of two contributions: one consequential from short-range forces between all species and other from long-range ion-ion interactions [33]. The non-random two liquid (NRTL) model was used to represent the short-range contribution and the Pitzer-Debye-Huckel model for the long-range contribution. It should be noted that the reference state of the first term

is the infinitely diluted aqueous solution and for the second term it is the infinite dilution in the mixed solvent. To correct the differences between reference states, the Born term is also added for mixed solvents.

Taking into account all terms, the total excess Gibbs energy can be expressed as follows:

$$\frac{G^E_{tot}}{RT} = \frac{G^{E,PDH}}{RT} + \frac{G^{E,Born}}{RT} + \frac{G^{E,lc}}{RT} \qquad (2.25)$$

Where $G^{E,PDH}$ is contribution of the long-range forces, $G^{E,lc}$ short-range forces and $G^{E,Born}$ of the Born term.

The activity coefficient of any species can be calculated as partial derivation of the excess Gibbs energy with respect to molar amount:

$$ln\gamma_i = \frac{1}{RT}\left[\frac{\partial(n_i G^E_{tot})}{\partial n_i}\right]_{T,P,n_{j\neq i}} \quad i,j = m,c,a \qquad (2.26)$$

Where *m*, *c* and *a* denote molecular, cationic and anionic species.

2.10.2.1 Long-range contribution

The first term in equation (1.25) can be expressed through the Pitzer-Debye-Huckel formulation:

$$\frac{G^{E,PDH}}{RT} = -\sum_k x_k \left(\frac{1000}{M_s}\right)^{\frac{1}{2}} \left(\frac{4A_\phi I_x}{\rho}\right) ln(1+\rho I_x^{0.5}) \qquad (2.27)$$

Where ρ is so-called "closest approach" parameter, M_s is molecular mass of the solvent. A_ϕ represents the Debye-Huckel parameter and I_x is the ionic strength on mole fraction scale, which can be decribed by the equation (2.28) and (2.29) respectively.

$$A_\phi = \frac{1}{3}\left(\frac{2\pi N_A d_s}{1000}\right)^{0.5} \left(\frac{e^2}{\varepsilon_s kT}\right)^{1.5} \qquad (2.28)$$

Where N_A is Avogadro number, d_s is solvent density, *e* is electron charge, ε_s is dielectric constant of water, k is Boltzmann constant.

$$I_x = 0.5\sum_i x_i z_i^2 \qquad (2.29)$$

Where x_i is mole fraction of component *i* and z_i is charge of component *i*.

2.10.2.2 Born correction

As already mentioned before, Born term accounts for the change in reference state for ions from infinitely diluted solution in water to infinitely diluted solution in amine-water mixture. This term mainly corrects the difference between the dielectric constant of water and that of the mixed solvent. The excess Gibbs energy can be described as follows:

$$\frac{G^{E,Born}}{RT} = \left(\frac{e^2}{2kT}\right)\left(\frac{1}{\varepsilon_m} - \frac{1}{\varepsilon_w}\right)\sum_i \frac{x_i z_i^2}{r_i} 10^{-2} \qquad (2.30)$$

Where $\varepsilon_m$is the dielectric constant of mixed solvent and r_i is Born radius.

2.10.2.3 Short-range contribution

The most important interactions in acid-gas treating by electrolyte solutions are local short-range interactions. The excess Gibbs energy expression for aqueous multicomponent electrolyte systems are defined as follows:

$$\frac{G^{E,lc}}{RT} = \sum_m X_m \frac{\sum_j X_j G_{jm}\tau_{jm}}{\sum_k X_k G_{km}} + \sum_c X_c \sum_{a'} \left(\frac{X_{a'}}{\sum_{a''} X_{a''}}\right) \frac{\sum_j G_{jc,a'c}\tau_{jc,a'c}}{\sum_k X_k G_{kc,a'c}} + \sum_a X_a \sum_{c'} \left(\frac{X_{c'}}{\sum_{c''} X_{c''}}\right) \frac{\sum_j G_{ja,c'a}\tau_{ja,ca}}{\sum_k X_k G_{ka,c'a}} \quad (2.31)$$

Some terms used in the equation (2.31) are explained by the next equations:

$$G_{cm} = \frac{\sum_a X_a G_{ca,m}}{\sum_{a'} X_{a'}} \qquad G_{am} = \frac{\sum_c X_c G_{ca,m}}{\sum_c X_{c'}} \quad (2.32)$$

$$\alpha_{cm} = \frac{\sum_a X_a \alpha_{ca,m}}{\sum_{a'} X_{a'}} \qquad \alpha_{am} = \frac{\sum_c X_c \alpha_{ca,m}}{\sum_c X_{c'}} \quad (2.33)$$

Where effective mole fraction $X_j = x_j C_j$ ($C_j = z_j$ for ions and C_j = unity for molecules). G and τ are local binary quantities related to each other by non-randomness factor α.

$$G_{jc,a'c} = exp\left(-\alpha_{jc,a'c}\tau_{jc,a'c}\right) \qquad G_{ja,c'a} = exp\left(-\alpha_{ja,c'a}\tau_{ja,c'a}\right) \quad (2.34)$$

$$G_{im} = exp(-\alpha_{im}\tau_{im}) \qquad G_{ca,m} = exp\left(-\alpha_{ca,m}\tau_{ca,m}\right) \quad (2.35)$$

$$\tau_{ma,ca} = \tau_{am} - \tau_{ca,m} + \tau_{m,ca} \qquad \tau_{mc,ac} = \tau_{cm} - \tau_{ca,m} + \tau_{m,ca} \quad (2.36)$$

2.11 Test of thermodynamic consistency

To assess the accuracy of the used experimental VLE data, test of thermodynamic consistency has to be carried out. The most commonly used test is the integral test proposed by Herington [34]. This test is based on the Gibbs-Duhem equation and provides so-called area test of the phase equilibrium data. The general form of Gibbs-Duhem equation can be defined as follows:

$$\sum x_i d\ ln\gamma_i = -\frac{\Delta V}{RT} dP + \frac{\Delta H}{RT^2} dT \quad (2.37)$$

Where ΔV represents molar volume of mixing and ΔH molar enthalpy of mixing.

It is very important that the experimental data satisfy this test with a defined accuracy. The accuracy requirements depend on the type of data. Phase equilibrium data are usually measured under isothermal or isobaric conditions. In the case of isothermal data, the integral form of equation (2.37) becomes:

$$\int_0^1 ln\frac{\gamma_1}{\gamma_2} dx_1 = -\int_0^1 \frac{\Delta V}{RT} dP \quad (2.38)$$

Usually, the integration expression on the right hand side of equation (2.38) can be neglected because of the very low values as reported by Kurihara [35]. Based on this assumption, equation (2.38) can be written as follows:

$$\int_0^1 ln\frac{\gamma_1}{\gamma_2} dx_1 = 0 \quad (2.39)$$

For isobaric data, the next correlation is applied:

$$\int_0^1 ln\frac{\gamma_1}{\gamma_2} dx_1 = -\int_0^1 \frac{\Delta H}{RT^2} dT \quad (2.40)$$

In this case, the right hand term of equation (2.40) cannot be neglected because of its high values. Since experimental data of the heat of mixing variation with temperature and composition are rarely available, Harington provided an empirical estimation of the right-side integral by the use of total boiling range of the mixture:

$$-\int_0^1 \frac{\Delta H}{RT^2}dT = J = 1.5\left|\frac{T_{max}-T_{min}}{T_{max}}\right| \quad (2.41)$$

Where T_{min} and T_{max} are boiling points of more and less volatile component.

A theoretically simple technique to test the data is by plotting the dependence of natural logarithm of the activity coefficients ration $ln\frac{\gamma_1}{\gamma_2}$ versus liquid mole fraction of the component x_1. The deviation of areas above and below x axis can be defined as follows:

$$\overline{D} = \frac{|A-B|}{A+B} \quad (2.42)$$

The isothermal VLE data can be considered as a consistent when $\overline{D}$ < 0.1, while isobaric data when $\overline{D} - J$ < 0.1 [34]. Graphical representation of the described thermodynamic test is shown on Figure 2.9.

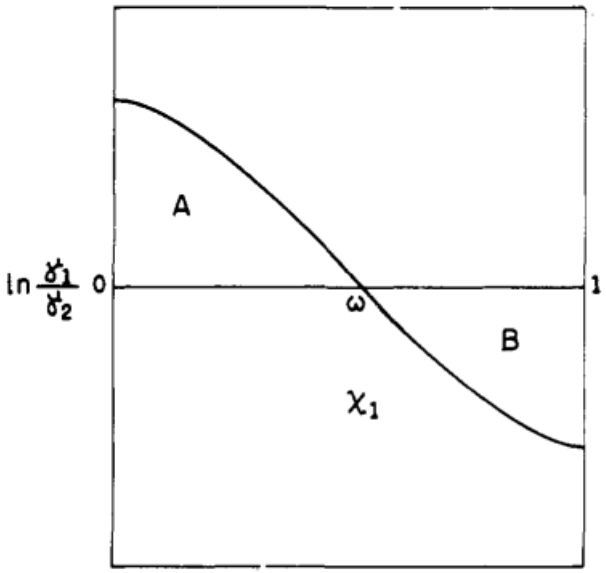

Figure 2.9 Illustration of thermodynamic consistency test

3 Aim of the work

- Experimental estimation of the solvent volatility.
- Experimental estimation of the vapor-liquid equilibrium of the AP-H_2O-CO_2 system.
- Experimental estimation of the heat of absorption of CO_2 by AP solution.
- To collect all available experimental data from the literature needed for modelling of the vapor-liquid equilibrium.
- To model the vapor-liquid equilibrium of binary AP-water system using NRTL-framework in MATLAB programming language.
- To evaluate the NRTL parameters and perform thermodynamic analysis of VLE.
- To extend the VLE model including CO_2 using the eNRTL-model to describe the component activities. The final model should be able to describe the ternary AP-H_2O-CO_2 system.

4 Work methodology

4.1 Binary system equilibrium description methodology

The main objective in the first part of this work was to model the vapor-liquid equilibrium of the binary alkanolamine (AP)-water system. Modelling itself is a very useful tool for understanding and prediction of the studied system phase behavior. In the case of the unloaded aqueous AP system, the degree of dissociation is very low and the presence of ions has been neglected. In this way, we have used the NRTL model for calculation of the components activity coefficients which is described in section 2.10.1. For calculation of the activity coefficients we have used two reference states in this work: pure component reference state (symmetrical approach) and infinite dilution state (asymmetric approach). The first case is applicable for liquids, both solutes and a solvent, assuming that the activity coefficient of each component is approaching unity when its mole fraction is equal to one and leads to an ideal solution in terms of the Raoult's law:

$$\gamma_i \to 1 \text{ as } x_i \to 1 \qquad (4.1)$$

The second case is based on the Henry's law and is applicable for solids and gases as pure components at the system temperature and pressure. According to this reference state, the activity coefficient is approaching unity as the mole fraction of these molecular and ionic solutes is equal to zero:

$$\gamma_s \to 1 \text{ as } x_s \to 0 \qquad (4.2)$$

As most of the models, the NRTL model has adjustable parameters (see section 2.10.1) which can be fitted against experimental data. These parameters are the binary interaction parameters and their calculation has an important role in the parameters regression of the more complex ternary CO_2-AP-water system. To solve this problem, four main steps were considered:

1. Gathering of all available experimental data from the literature covering a wide range of temperatures, pressures and compositions.
2. Update the NRTL model suitable for our optimization problem.
3. Create an algorithm that can be used for regression of the NRTL parameters.
4. Test the thermodynamic consistency of the used experimental data in calculation of the activity coefficients and correlate different thermodynamic properties to check the accuracy of the proposed model.

A complete list of all sets of data used in this work is presented in Table 4.1. In order to provide quality interaction parameters, it was very important to collect different type of data. We can noticed that for the binary AP-water system were available VLE data and thermal data such as: excess enthalpy and heat capacity.

Table 4.1 Summarization of all available data used in model parameters fitting

Experimental type data	Collected data	Experimental conditions	Number of points	Refer	Remarks
VLE	*PTxy* Isothermal	T = 313 K, 333 K, 353 K, 373 K	44	[a]	Ebulliometer
		x_{AP} = 0 to 0.2			
		y_{AP} = 0 to 0.2			
		P = 10-1000 mbar			
	PTx Isothermal	T = 348 K, 358 K, 368 K	33	[37]	
		x_{AP} = 0 to 1			
		y_{AP} = 0 to 1			
	PTx Isobaric	T = 356-430 K	33	[37]	
		x_{AP} = 0 to 1			
		y_{AP} = 0 to 1			
		P = 533 mbar, 667 mbar, 800 mbar			
Calorimetric	HE Excess enthalpy of mixing	T = 298 K, 313 K, 323 K	33	[38]	Calorimeter
		x_{AP} = 0 to 1			
	cpE	T = 303-353 K	99	[38]	
	Excess heat capacity	x_{AP} = 0 to 1			

[a] - in-house vapor-liquid equilibrium data;

Very big impact on the accuracy of the model has also the pure component vapor pressure. In the case of AP, there was a lack of experimental vapor pressure measurements and the only available data were the published Antoine coefficients. Antoine coefficients used in this work were taken from the DECHEMA database and are presented in Table 4.4.

In the second step, as suggested by Austgen, et al and Hessen, et al. [39, 40], we defined the interaction parameters as temperature dependent:

$$\tau_{12} = a_{12} + \frac{b_{12}}{T(K)} \quad (4.3)$$

$$\tau_{21} = a_{21} + \frac{b_{21}}{T(K)} \quad (4.4)$$

$$\alpha_{12} = \alpha_{21} = 0.2 \quad (4.5)$$

The non-randomness parameter was fixed at 0.2 as proposed by Chen, et al. [32].

To obtain these binary parameters, it is necessary to have a suitable objective function that will be minimized. In the next step, we have defined the objective function as a sum of the squares of differences between the experimental and calculated values of the total pressure, temperature and excess enthalpy as follows:

$$F = \sum\sum \left(\frac{Y^{exp} - Y^{cal}}{Y^{exp}} \right)^2 \quad (4.6)$$

An optimization routine *fminsearch* was used for the minimization of the objective function. The proposed algorithm for solving of this optimization problem is given in Figure 4.1. The entire modeling was performed in the MATLAB programming language.

In the last step, area tests of the phase equilibrium data were performed as described in section 2.11. The average absolute relative deviation (*AARD*) between the model representation and the experimental data was calculated to examine the accuracy of the developed model using the equation [41]:

$$AARD\ Y\ \% = \frac{100}{N} \sum_{i=1}^{N} \left| \frac{Y_i^{exp} - Y_i^{cal}}{Y_i^{exp}} \right| \quad (4.7)$$

Where N represents the total number of data points and the variable *Y* indicates the total pressure, temperature or excess enthalpy. Results of the performed consistency tests are given in the Table 5.1.

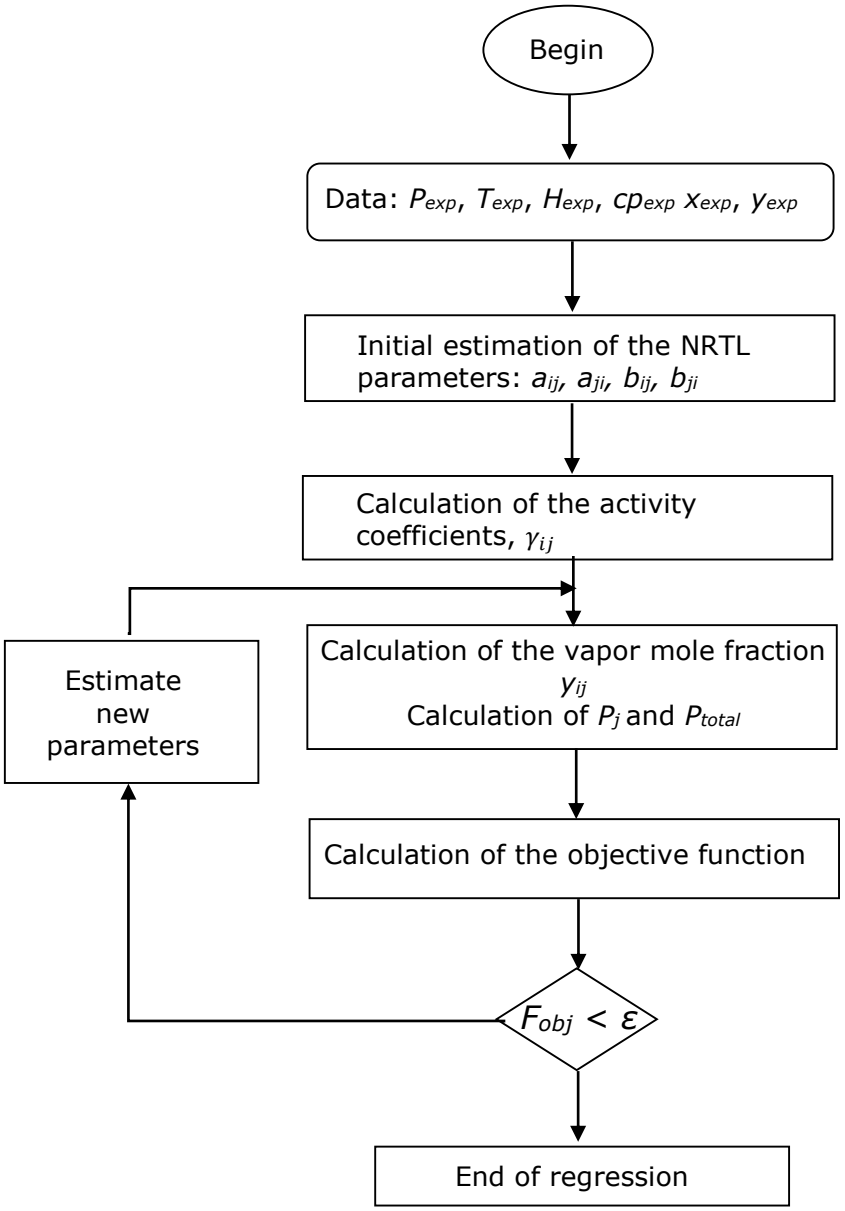

Figure 4.1 Optimization algorithm for the model parameters

4.2 Ternary system equilibrium description methodology

The ternary AP-H_2O-CO_2 system is a reactive system and both chemical and phase equilibrium have to be included in the modeling process. The reaction mechanism of this system was explained in section 2.8. Nine species are present in the system: three molecules (AP, H_2O, CO_2), two cations (APH^+, $H3O^+$) and four anions (OH^-, HCO_3^-, CO_3^{2-}, $APCO_2^-$). The electrolyte NRTL model was chosen for calculation of the activity coefficients of the species (see section 2.10.2), while the Peng Robinson equation of state was used for description of the vapor phase.

The equilibrium description methodology of the ternary system was the same as for the binary system. For fitting the eNRTL parameters, experimental VLE data reported as a function of the CO_2 partial pressure with the temperature and loading were collected and are shown in Table 4.2. The pure component properties and correlations used in this work were taken from the Aspen Plus database and are reported in Tables 4.3, 4.4, 4.5 and 4.6.

Table 4.2 Summary of all available data used in the model parameters fitting

Experimental type data	Collected data	Experimental conditions	Number of points	Refer
VLE	P_{CO2}, T, [AP], α	T = 313 K	22	[43]
		[AP] = 3.9, 5 M		
		α = 0.2 to 0.53		
		P_{CO2} = 0.0047 to 4.2 kPa		
		T = 293 K, 313 K, 333 K, 353 K, 373 K	20	[44]
		[AP] = 7 M		
		α = 0.33 to 0.59		
		P_{CO2} = 0.01 to 42.1 kPa		
		T = 313 K, 343 K, 373 K, 393 K	101	[45]
		[AP] = 2, 4, 5 M		
		α = 0.2 to 1.02		
		P_{CO2} = 2.5 to 705 kPa		
		T = 298 K, 313 K, 323 K, 333 K	60	[46]
		[AP] = 1.3, 2 M		
		α = 0.64 to 1.20		
		P_{CO2} = 13 to 1291 kPa		

Table 4.3 Pure component properties [47]

Properties	H_2O	CO_2	AP
***MW* [g/mol]**	18.015	44.009	75.111
T_c [K]	647.108	304.179	708
P_c [kPa]	22071.457	7381.833	6009.301
V_c [m^3/kmol]	0.0559	0.0943	0.242
ω [-]	0.344	0.225	0.381
Z_c [-]	0.2297	0.275	0.247
Brelvi-O'Connell parameter	0.0464	0.0939	

Table 4.4 Antoine equation coefficients of molecular species; [a] - taken from Aspen Plus database [47]; [b] - taken from DECHEMA database [37];

Coefficient	H_2O [a]	CO_2 [a]	AP [b]
A	72.55	72.82912	13.0651
B	-7206.7	-3403.28	-4354.4
C	0	0	358.835
D	0	9.49×10-3	0
E	-7.1385	-8.56034	0
F	4.05×10^{-6}	2.91×10^{-16}	0
G	2	6	0

Table 4.5 Dielectric constants of pure components [48]

Species	a_1	b_1
H_2O	78.65	31989
AP	21.9957	8992.68

Table 4.6 Correlations used in the ternary eNRTL model [47]

$\ln(P_i^{\circ}/Pa) = A + \frac{B}{T(K)+C} + D(T/K) + Eln(T/K) + F(T/K)^G$	(4.8)
$\varepsilon = a_1 + b_1/T(K)[1/T(K) - 1/298.15]$	(4.9)
$\ln K_i\,(mole\ fraction) = a + b/T(K) + C\ln T(K) + D\,T(K)$	(4.10)
$\ln H_{CO2}^{\infty}(MPa) = -6.8346 + \frac{1.2817*10^4}{T} - \frac{3.7668*10^6}{T^2} + \frac{2.997*10^8}{T^3}$	(4.11)
$\frac{\partial\, lnK_i}{\partial\, T} = \frac{\Delta H_r}{R\,T^2}$	(4.12)

The chemical equilibrium constants expressed on the mole fraction basis are given in Table 4.7. The protonation constant of AP (K_4) was fitted from the literature data [49] while the equilibrium constant for carbamate formation (K_5) was regressed together with the eNRTL parameters. The rest of the equilibrium constants were taken from the Aspen Plus database.

Table 4.7 Chemical equilibrium constants

	A	*B*	*C*	*D*	Range [K]	Refer.
K_1	-9.870	-6693.14	1.0358	-0.00179		This work
K_2	0.921	18.996	2631.983	0		This work
K_3	231.465	-12092.1	-36.7816	0	237-498	[50]
K_4	132.899	-13445.9	-22.4773	0	237-498	[50]
K_5	216.049	-12431.7	-35.4819	0	237-498	[50]

For the regression of the interaction parameters, temperature dependence form was used as follows:

$$\tau_{m,ca} = a_{m,ca} + \frac{b_{m,ca}}{T(K)} \quad (4.13)$$

$$\tau_{ca,m} = a_{ca,m} + \frac{b_{ca,m}}{T(K)} \quad (4.14)$$

$$\alpha_{H2O,ca} = 0.2 \quad (4.15)$$

$$\alpha_{ca,CO2/AP} = 0.1 \quad (4.16)$$

According to Chen, et al. [32], the non-randomness values for the molecule-ion pair were set as default values (see equations 4.15 and 4.16).

A simple optimization algorithm for ternary system is shown in Figure 4.2. In this work a rigorous thermodynamic modeling of the ternary system VLE was performed using the model of Diego Di. D Pinto and Juliana Monteiro, Phd students at the Norwegian University of Science and Technology (NTNU) at Trondheim and an optimization routine created in this work. The in-house vapor-liquid equilibrium model was used as the coding of amine-CO_2-water system with numerous adjustable parameters is too complex to be coded in the time available. For this purpose, Particle Swarm Optimization (PSO) algorithm was implemented. The advantage of this routine is that it does not require initial estimates to run the optimization, but is initialized randomly. A detailed overview of the PSO method can be found in the literature [51, 52, 53]. The values of the PSO parameters used in this work are given in Table 4.8 and are based on a study by Clerc and Kennedy [52]. The proposed algorithm for this optimization routine is shown in Figure 4.3.

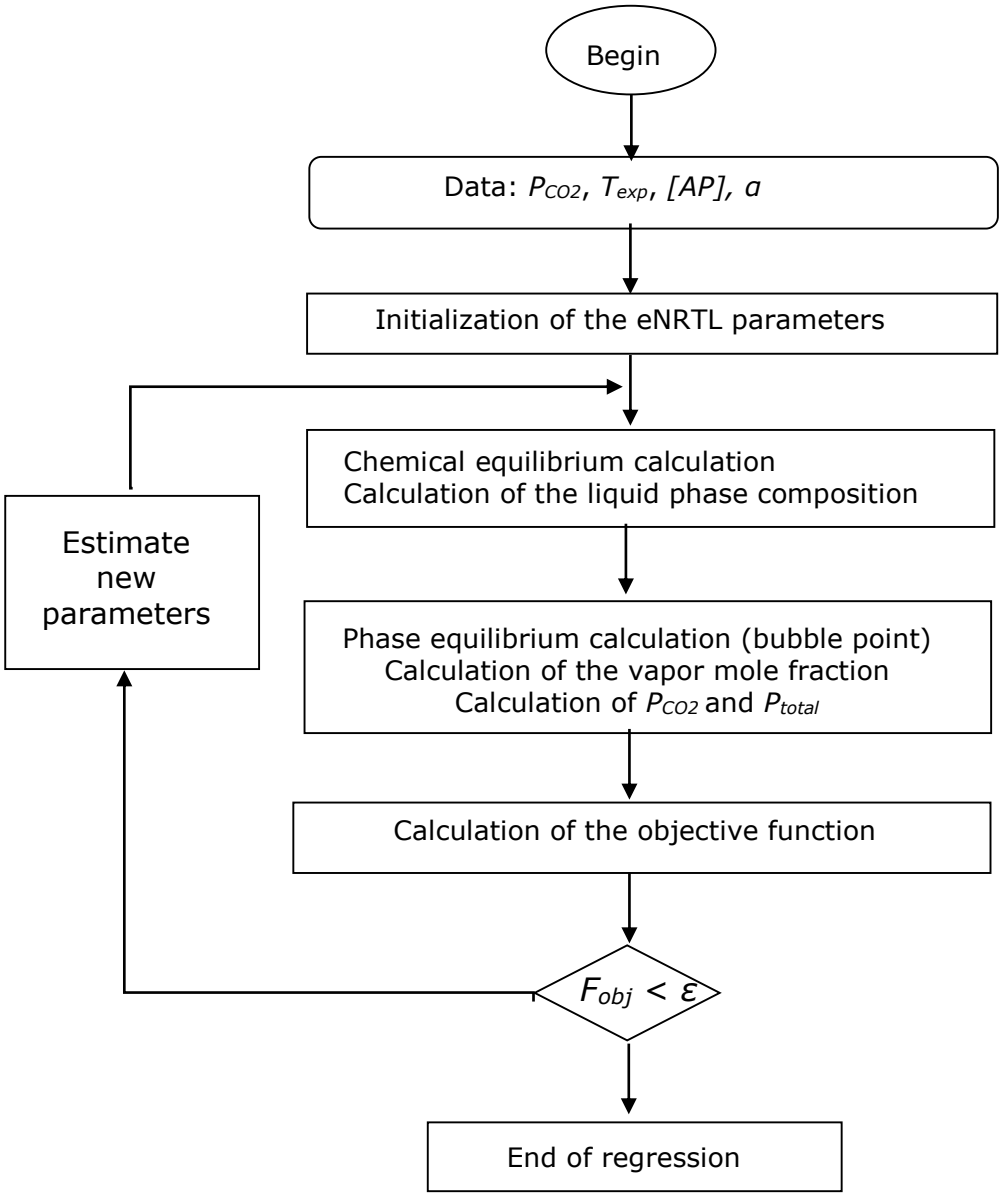

Figure 4.2 Optimization algorithm for the ternary AP-H_2O-CO_2 system

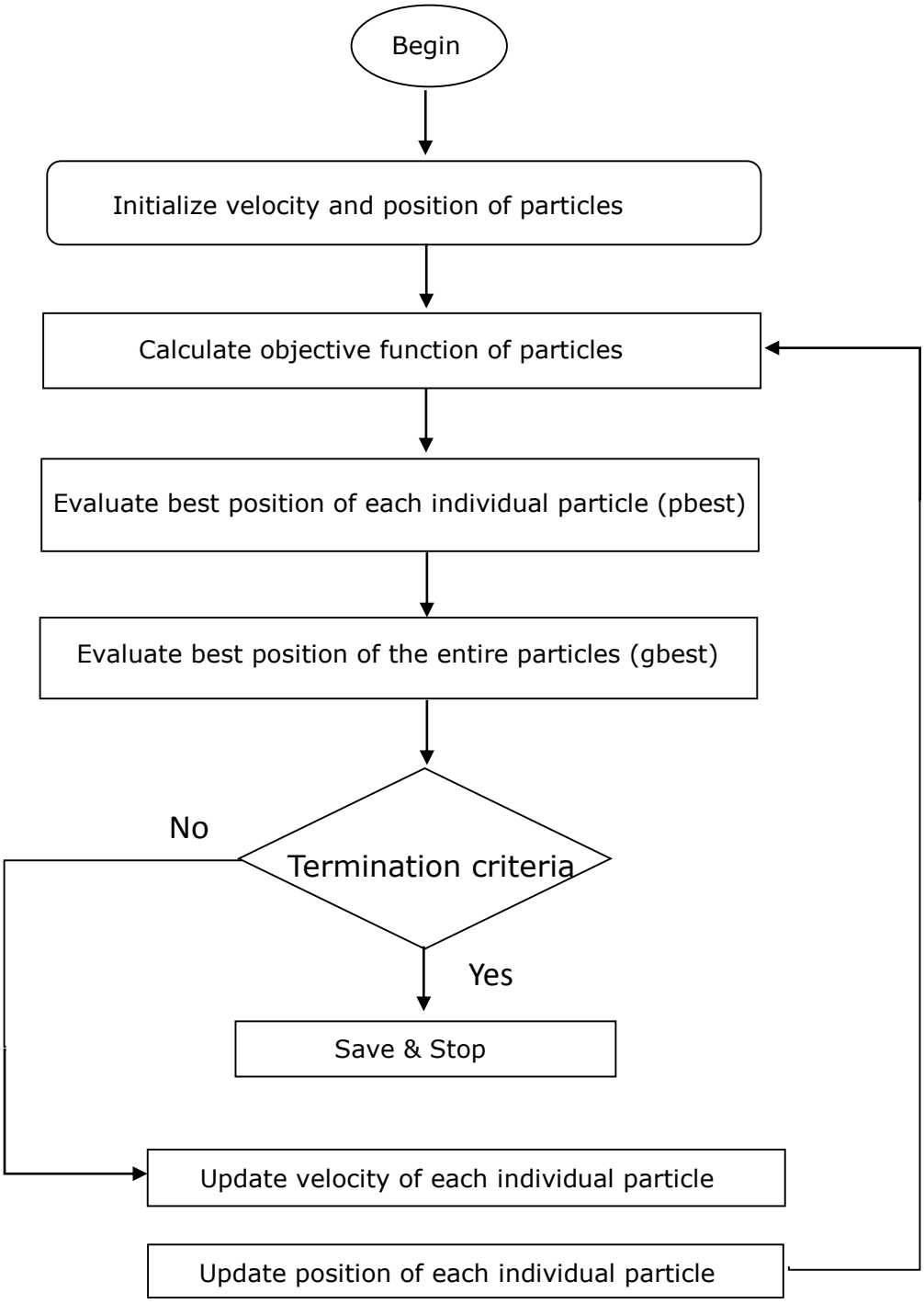

Figure 4.3 Optimization procedure using the PSO algorithm [54]

Table 4.8 PSO parameters [52]

Parameter	Value
Tolerance	$1e^{-4}$
Maxiter	300
Inertia weight (ω)	0.7298
$\boldsymbol{\Phi_1}$	1.4962
$\boldsymbol{\Phi_2}$	1.4962
Swarm size	40

The PSO optimization routine was used to minimize the objective function defined as the sum of square of the error between the experimental and calculated CO_2 partial pressure values:

$$F = \sum\sum\left(\frac{P_{CO2}^{exp} - P_{CO2}^{cal}}{P_{CO2}^{exp}}\right)^2 \qquad (4.17)$$

5 Results and discussion

5.1 Results of binary phase equilibrium data simulation

The results presented in this section are based on the fitting procedure described in the previous section and the data sets summarized in Table 4.1. Due to the large number of obtained dependencies, complete overview of the results is provided in Appendix 1. We can notice that the model results are in a perfect agreement with the experimental data with the accuracy of the model given in section 5.1.1 and the optimized parameters are of good quality.

In Figure 5.1 - a), b) are presented the reported ebulliometric *PTxy* data from NTNU (in-house VLE data) together with the computed values of the total pressure, while Figure 5.2 shows the results of calculated components activity coefficients of aqueous AP system. Model shows a very good representation of data with an *AARD* values of 0.51% and 0.88 % for the total pressure at 373 K and 353 K, respectively.

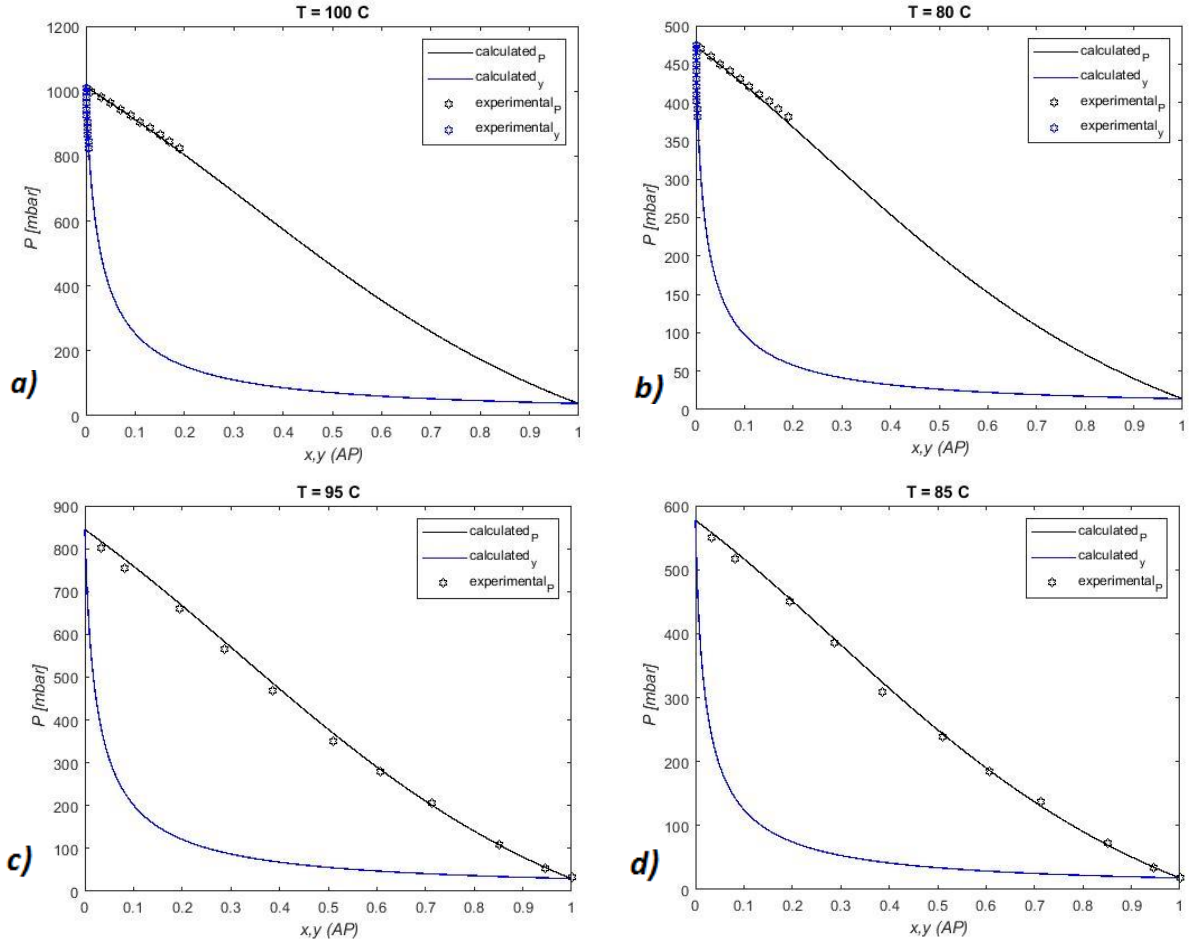

Figure 5.1 Isothermal Pxy diagram for binary AP - water system at: a) 373 K, b) 353 K (Points from the in-house VLE data), c) 368 K, d) 358 K (Points [37]). Black solid lines - calculated boiling curves; Blue solid lines - calculated dew point curves; * - Experimental data points;

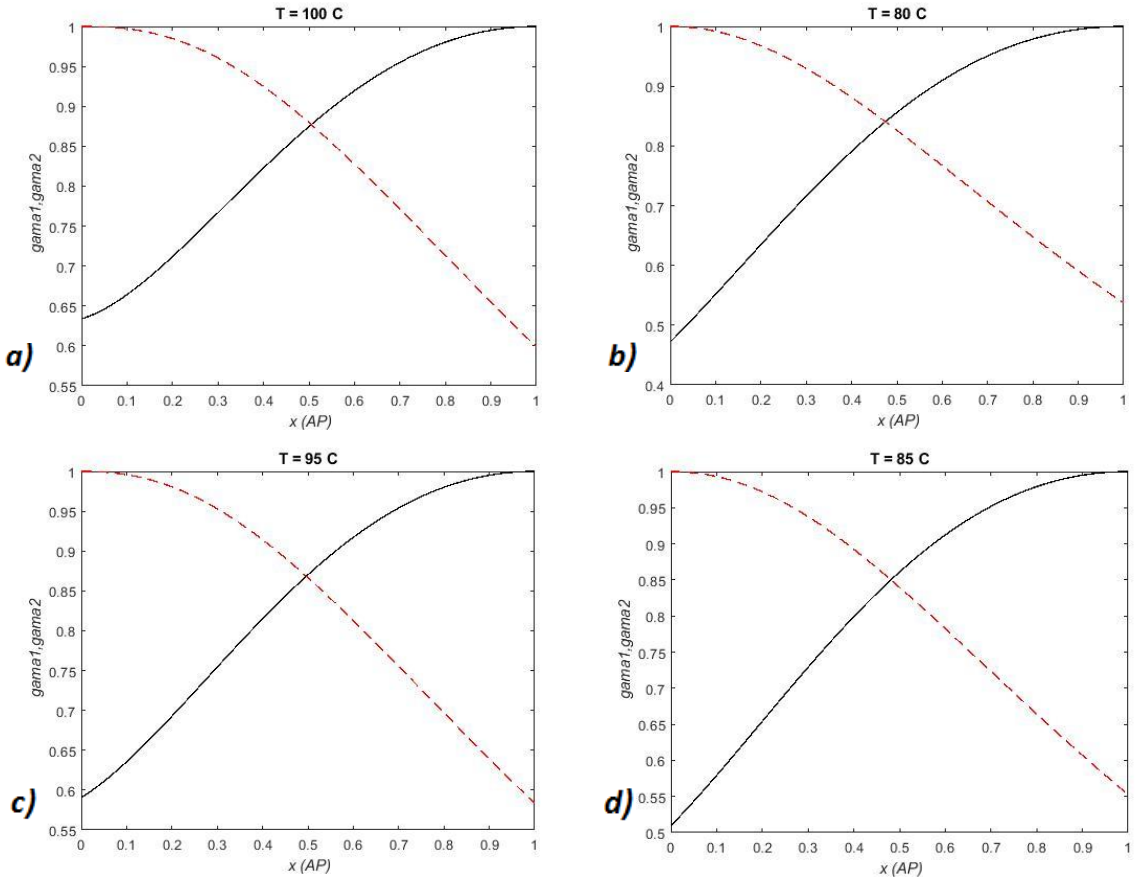

Figure 5.2 Activity coefficients of AP at: a) 373 K, b) 353 K (Points from the in-house VLE data), c) 368 K, d) 358 K (Points [37]). Black solid lines - γ_{AP}; Red dashed lines - γ_{Water}

As we can see, VLE data were measured only up to 20% mole fraction of AP in water. Since in practice an acid gas - alkanolamine system contains less than 20% mole fraction of alkanolamine, it is very important to accurately represent the activity coefficients in this region. However, for the best fit of the data, it is necessary to cover the whole range of AP concentrations. A very good representation of the isothermal *PTx* data can be notice in Figure 5.1 – c), d) with the *AARD* values of 3.1 % and 2.5 % for the total pressure at 368 K and 358 K, respectively. The calculated activity coefficients for this set of data are shown in Figure 5.2 – c), d).

The representation of the model for the isobaric *PTx* data is shown in Figure 5.3. From the figure it can be seen that the data and model are in excellent agreement with the *AARD* values of 0.58 %, 0.47 % and 0.44 % for the points of bubble temperature at 533 mbar, 667 mbar and 800 mbar, respectively. Figure 5.4 and 5.5 show the mole fraction dependencies of the experimental and calculated colorimetric properties: excess enthalpy and excess heat capacity at various temperatures. The excess molar enthalpy shows negative values at all temperatures as expected. This indicates heat evolution on mixing of AP with water due to the strong interaction between the *-OH* group of water molecules and *-NH_2* group of AP molecules. The fit of data is good with a small deviations in the region where the released heat values are the highest (from 0.3 to 0.5 AP composition in the liquid phase) with the *AARD* values of 5.3 %, 2.7 % and 5.9 % at 298 K, 313 K and 323 K, respectively.

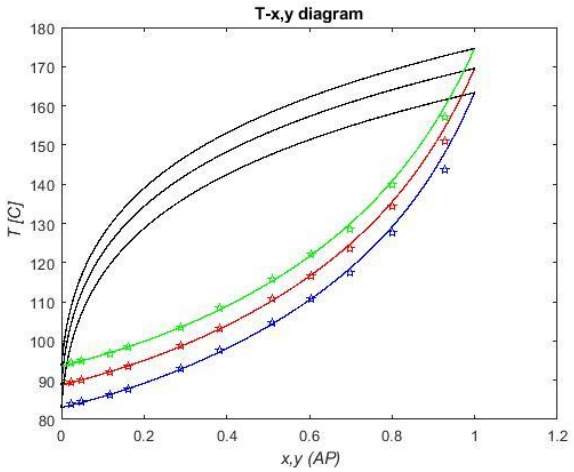

Figure 5.3 Isobaric Txy data for binary AP-water system at: 533 mbar (blue color), 667 mbar (red color), 800 mbar (green color); Solid lines – NRTL model; * - Experimental data points [37]

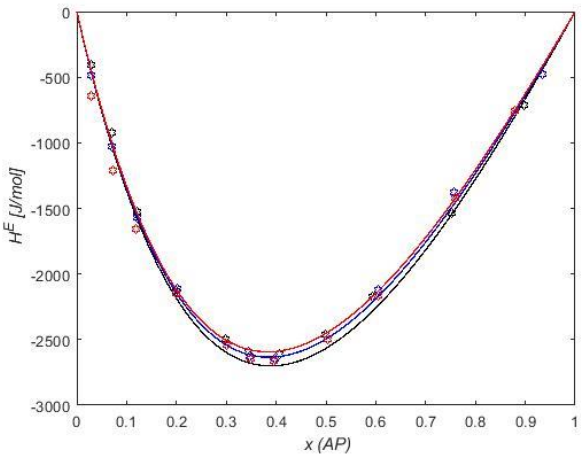

Figure 5.4 Excess enthalpy dependence of the AP-water mixture composition at: 298 K (black color), 313 K (blue color), 323 K (red color); Solid lines - NRTL model, * - Experimental data points [38]

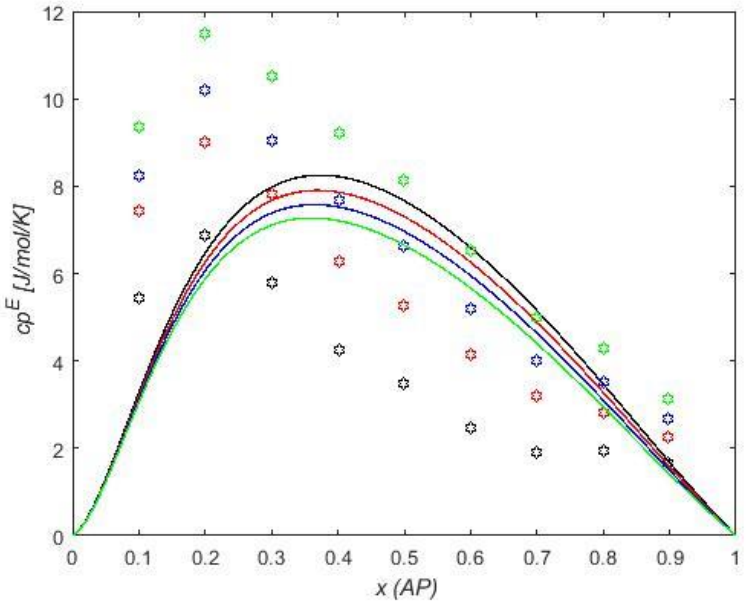

Figure 5.5 Excess heat capacity dependence of the AP-water mixture composition at: 303 K (black color), 308 K (red color), 313 K (blue color), 323 K (green color); Solid lines - NRTL model; * - Experimental data points [38]

The only not reasonable model prediction was noticed for the excess heat capacity variation with the mixture composition with the *AARD* value of 56.7 %. As we can see, the model shows a decrease in excess heat capacity with increasing temperature, while the data show the opposite trend. This behavior was observed also in other studies [36, 42]. For this reason, the excess heat capacity was not used in the parameters fitting.

All of the VLE data satisfy the area tests of thermodynamic consistency. The results of some tests are shown in Figure 5.6. Calculated areas are presented in Table 5.1.

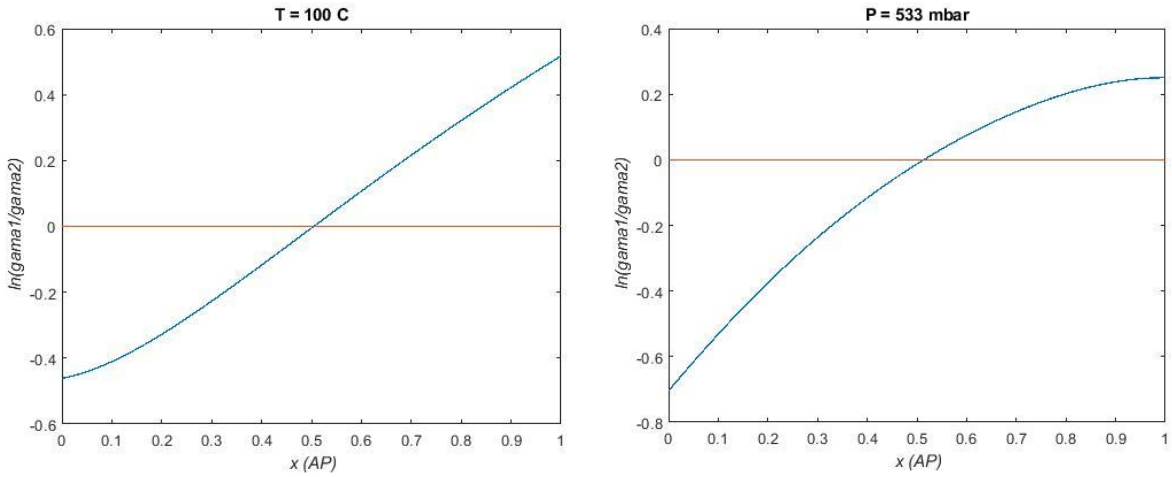

Figure 5.6 Test of thermodynamic consistency for binary AP-water system at: a) isothermal condition, b) isobaric condition

Table 5.1 Calculated area tests of thermodynamic consistency for isobaric (D) and isothermal data (D-J); [a] - Points from in-house VLE data; [b] - Points from DECHEMA database [37];

***T* [K]**	**313** [a]	**333** [a]	**353** [a]	**373** [a]	**348** [b]	**358** [b]	**368** [b]
D	-3076.3	-8635.6	-23005.1	-2280.5	-3391.5	-53.8	-2730.1
	P = 53.3 kPa [b]			*P* = 66.7 kPa [b]		*P* = 80 kPa [b]	
D-J	-4.21			-4.02		-3.86	

Regressed interaction parameters for binary AP-Water system are given in Table 5.2.

Table 5.2 Regressed binary interaction NRTL parameters

Parameters	a_{12}	a_{21}	b_{12}	b_{21}
AP-H_2O	-0.9199	5.3843	-440.1005	-989.2131

5.1.1 Accuracy of the model

A total of 77 data points for total pressure, 33 data points for excess enthalpy and 33 data for points of bubble temperature were used in this work for regression of the NRTL model parameters. Figures 5.7, 5.8 and 5.9 show a parity plot between experimental and model representation of the data. From these figures it can be seen that the model and experimental data are in excellent agreement with: *AARD* of 1.9 % for total pressure, *AARD* of 4.7 % for excess enthalpy and *AARD* of 0.5 % for the bubble point temperature data.

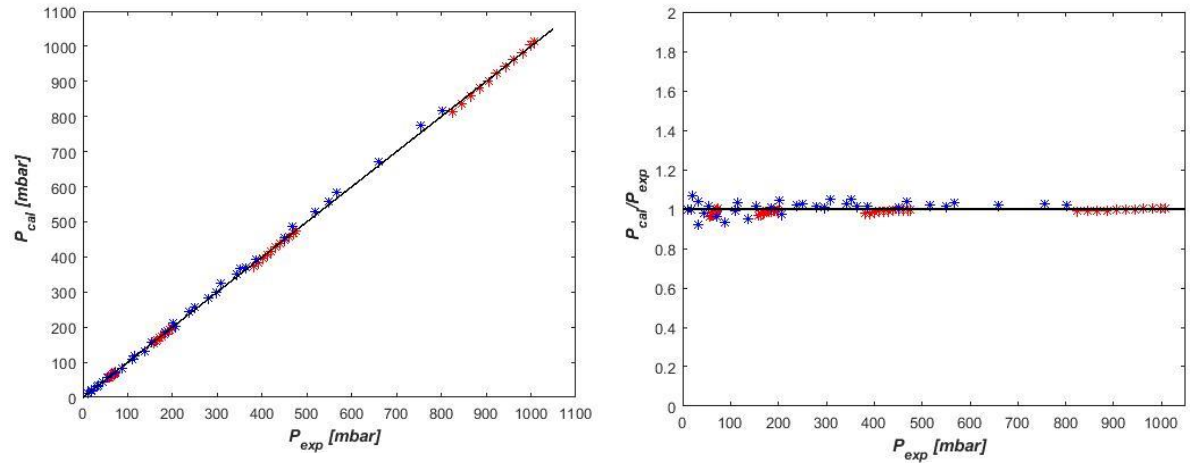

Figure 5.7 Parity plot between model representation and experimental total pressure data; Blue color – points from in-house VLE data; Red color – points from DECHEMA database [37]

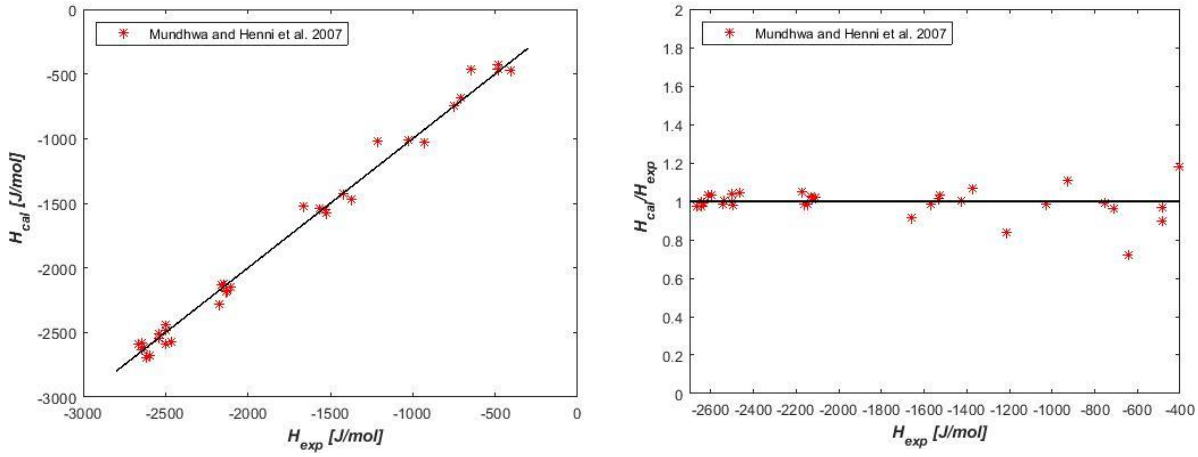

Figure 5.8 Parity plot between model representation and experimental excess enthalpy data

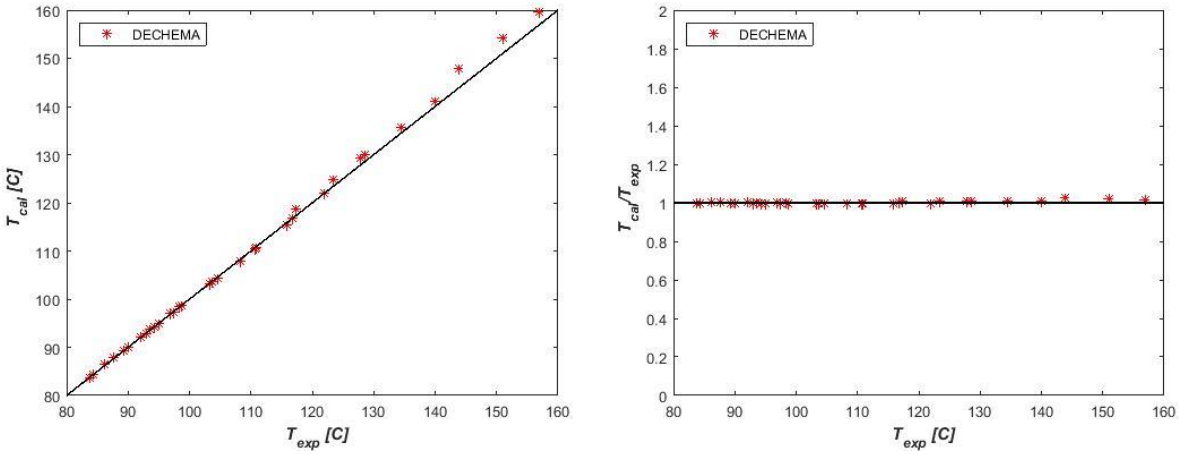

Figure 5.9 Parity plot between model representation and experimental points of bubble temperature data

5.2 Full model prediction of the ternary AP-H_2O-CO_2 system

As mentioned earlier, the eNRTL model consists of a large number of adjustable parameters. Based on sensitivity analyses for the parameter fitting problem performed by Austgen, et al. [55] and Rochelle, et al. [56], model parameters that are the most sensitive to the experimental data were identified. In this way, the non-sensitive parameters were set as default values taken from the Aspen Plus database. By fixing the values of the non-sensitive and previously calculated interaction parameters, optimization of the remaining parameters of the AP-H_2O-CO_2 system was performed and the results of this optimization procedure are shown in Table 5.3.

Table 5.3 ***Regressed eNRTL parameters; [a] - taken from Aspen Plus database [47]***

1	H_2O		4	H_3O^+		7	HCO_3^-
2	CO_2		5	APH^+		8	CO_3^{2-}
3	AP		6	OH^-		9	$APCO_2^-$
	a (-)		*b (K)*		*a (-)*		*b (K)*
Molecule - molecule parameters							
$a_{1,2}$	0 [a]	$b_{1,2}$	0	$a_{2,1}$	0 [a]	$b_{2,1}$	0
$a_{2,3}$	-2.82	$b_{2,3}$	1099.4	$a_{3,2}$	-5.56	$b_{3,2}$	259.00
Molecule - ions parameters							
$a_{1,4\text{-}6}$	8 [a]	$b_{1,4\text{-}6}$	0	$a_{4\text{-}6,1}$	-4 [a]	$b_{4\text{-}6,1}$	0
$a_{1,4\text{-}7}$	8 [a]	$b_{1,4\text{-}7}$	0	$a_{4\text{-}6,2}$	-8 [a]	$b_{4\text{-}6,2}$	0
$a_{1,4\text{-}8}$	8 [a]	$b_{1,4\text{-}8}$	0	$a_{4\text{-}6,3}$	9.37	$b_{4\text{-}6,3}$	-663.83
$a_{1,4\text{-}9}$	-0.39	$b_{1,4\text{-}9}$	712.84	$a_{4\text{-}7,1}$	-4 [a]	$b_{4\text{-}7,1}$	0
$a_{1,5\text{-}6}$	1.89	$b_{1,5\text{-}6}$	1188.64	$a_{4\text{-}7,2}$	-8 [a]	$b_{4\text{-}7,2}$	0
$a_{1,5\text{-}7}$	-0.35	$b_{1,5\text{-}7}$	393.53	$a_{4\text{-}7,3}$	0.101	$b_{4\text{-}7,3}$	1431.58
$a_{1,5\text{-}8}$	0.72	$b_{1,5\text{-}8}$	-204.26	$a_{4\text{-}8,1}$	-4 [a]	$b_{4\text{-}8,1}$	0
$a_{1,5\text{-}9}$	-2.93	$b_{1,5\text{-}9}$	-752.68	$a_{4\text{-}8,2}$	-8 [a]	$b_{4\text{-}8,2}$	0
$a_{2,4\text{-}6}$	15 [a]	$b_{2,4\text{-}6}$	0	$a_{4\text{-}8,3}$	0.81	$b_{4\text{-}8,3}$	-644.00
$a_{2,4\text{-}7}$	15 [a]	$b_{2,4\text{-}7}$	0	$a_{4\text{-}9,1}$	-0.59	$b_{4\text{-}9,1}$	1884.63
$a_{2,4\text{-}8}$	15 [a]	$b_{2,4\text{-}8}$	0	$a_{4\text{-}9,2}$	1.51	$b_{4\text{-}9,2}$	1719.60
$a_{2,4\text{-}9}$	3.41	$b_{2,4\text{-}9}$	1431.61	$a_{4\text{-}9,3}$	3.87	$b_{4\text{-}9,3}$	764.37
$a_{2,5\text{-}6}$	-0.018	$b_{2,5\text{-}6}$	1315.94	$a_{5\text{-}6,1}$	3.57	$b_{5\text{-}6,1}$	1583.02
$a_{2,5\text{-}7}$	1.29	$b_{2,5\text{-}7}$	-144.64	$a_{5\text{-}6,2}$	-0.68	$b_{5\text{-}6,2}$	2358.23
$a_{2,5\text{-}8}$	0.97	$b_{2,5\text{-}8}$	2063.45	$a_{5\text{-}6,3}$	8.32	$b_{5\text{-}6,3}$	-104.1
$a_{2,5\text{-}9}$	1.96	$b_{2,5\text{-}9}$	810.31	$a_{5\text{-}7,1}$	3.78	$b_{5\text{-}7,1}$	1258.36
$a_{3,4\text{-}6}$	10.39	$b_{3,4\text{-}6}$	432.19	$a_{5\text{-}7,2}$	-3.82	$b_{5\text{-}7,2}$	2317.41
$a_{3,4\text{-}7}$	2.30	$b_{3,4\text{-}7}$	1839.43	$a_{5\text{-}7,3}$	0.40	$b_{5\text{-}7,3}$	-77.72
$a_{3,4\text{-}8}$	-5.20	$b_{3,4\text{-}8}$	412.75	$a_{5\text{-}8,1}$	-0.44	$b_{5\text{-}8,1}$	-1753.51
$a_{3,4\text{-}9}$	4.31	$b_{3,4\text{-}9}$	568.62	$a_{5\text{-}8,2}$	-0.89	$b_{5\text{-}8,2}$	795.00
$a_{3,5\text{-}6}$	3.65	$b_{3,5\text{-}6}$	-18.39	$a_{5\text{-}8,3}$	-0.90	$b_{5\text{-}8,3}$	788.52
$a_{3,5\text{-}7}$	-1.61	$b_{3,5\text{-}7}$	-983.94	$a_{5\text{-}9,1}$	6.19	$b_{5\text{-}9,1}$	1757.02
$a_{3,5\text{-}8}$	3.06	$b_{3,5\text{-}8}$	268.73	$a_{5\text{-}9,2}$	3.89	$b_{5\text{-}9,2}$	1647.25
$a_{3,5\text{-}9}$	-1.58	$b_{3,995\text{-}9}$	476.06	$a_{5\text{-}9,3}$	2.23	$b_{5\text{-}9,3}$	921.61

The results from the experimental and calculated data of CO_2 partial pressure as a function of the CO_2 loading in the liquid phase and temperature are shown in Figures 5.10 to 5.14. It can be seen that the eNRTL model representation for all experimental data sets is reasonable with the accuracy of the model given in section 5.2.1. However, there was a lack of data which made the fitting procedure more difficult. Most of the VLE data were reported at a high CO_2 loading and no data were available to compare the representation of the CO_2 partial pressure at lower loadings.

Figure 5.10 shows the eNRTL model representation of the CO_2 partial pressure at AP initial concentration in the liquid phase of 7 M and equilibrium CO_2 loading from 0.3 to 0.6. The model slightly over-predicts the CO_2 partial pressure over the entire temperature range with the *AARD* values of 33.2 %. Figure 5.11 shows a good trend of data description at two AP initial concentrations: 3.9 M and 5 M with the *AARD* values of 15.6 % and 27 % respectively. From the figure it can be seen that the reported data correspond to lower CO_2 loadings, from 0.2 to 0.6. However, the data points in this region are quite close, which makes the model description difficult to follow.

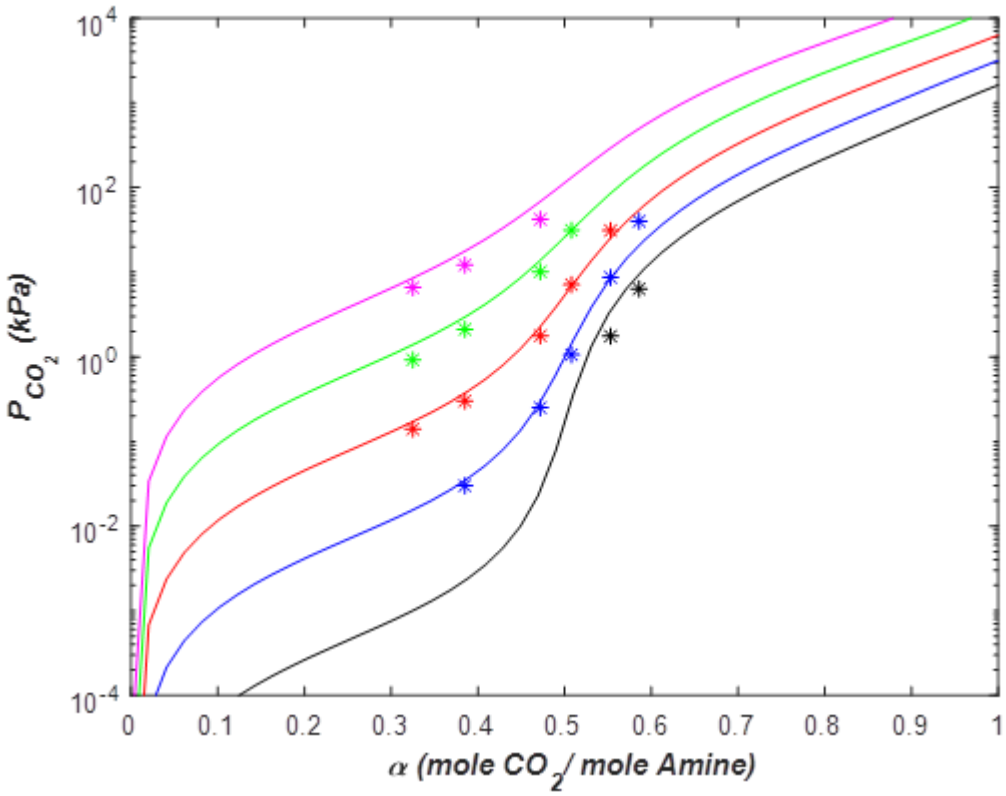

Figure 5.10 CO_2 partial pressure dependence as a function of loading at: 293 K (black color), 313 K (blue color), 333 K (red color), 353 K (green color), 373 K (pink color) and [AP] = 7 M; Solid lines – eNRTL model representation, *-Experimental data points [44]

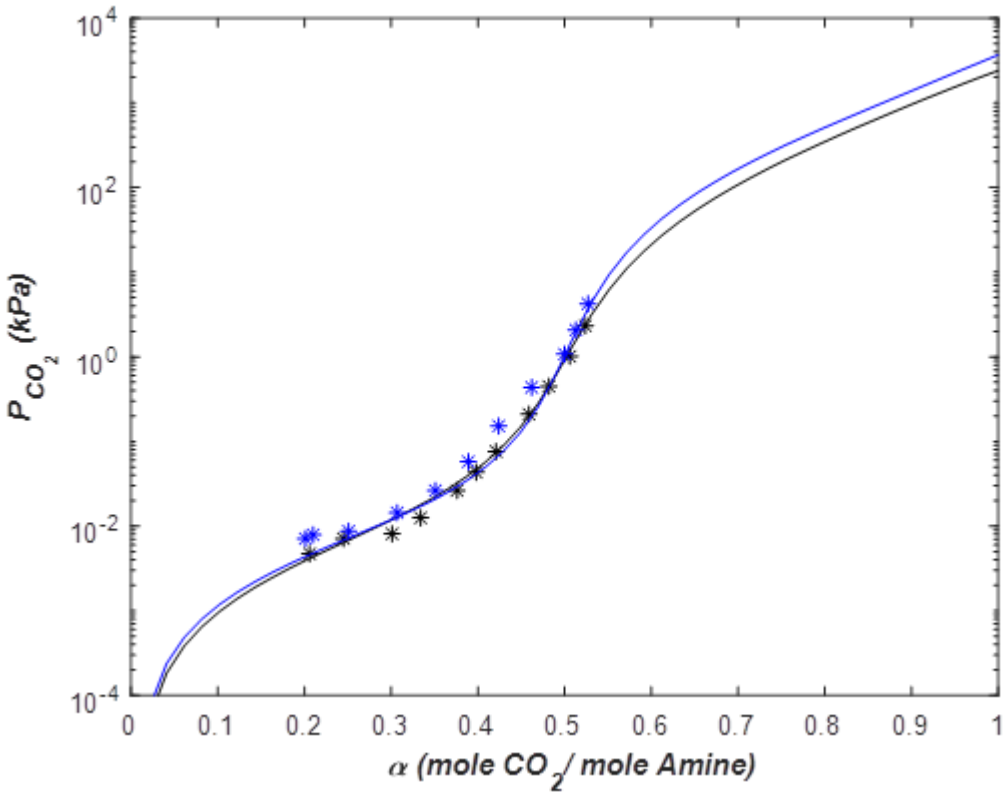

Figure 5.11 CO_2 partial pressure dependence as a function of loading at 313 K and [AP] = 3.9 M (black color), [AP] = 5 M (blue color); Solid lines - eNRTL model representation, * - Experimental data points [43]

For the AP initial concentration of 2 M, two sets of data are reported ([46], [45]) as shown in Figure 5.12 with the *AARD* values of 10.9% and 15.6 %, respectively. At higher CO_2 loadings, the experimental data are in good agreement with the computed ones for both sets of data over the entire temperature range, while at loadings lower than 0.6 there is a slight deviation between the experimental and simulated data. This trend can be seen in the following figures, where at loadings below 0.8 (see Figure 5.13) and 0.6 (see Figure 5.14), the model under-predicts the CO_2 partial pressure. Nevertheless, from these figures it can be seen that there is a lack of data for verification of the predictions of the model at lower CO_2 loadings. This shows the importance of having experimental data also within the CO_2 loading range from 0 to 0.6 in order to reach better accuracy of the model prediction. This lower CO_2 loading range is basically the most important area in the CO_2 capturing process. Moreover, neither total pressure nor N_2O solubility data are available. They would be of a great help improving this model. The N_2O analogy is usually used for measuring of the physical solubility of CO_2 in the aqueous alkanolamine system because the AP-CO_2 system is a reactive system. As already mentioned in section 2.9, the infinite dilution of CO_2 in water corresponds to the Henry's law constant (see also equation 4.11). This indirect measurement will help to calculate the apparent Henry's law constant for CO_2 in the mixed AP-water solvent and to increase the accuracy of the model. Calculated *AARD* values for CO_2 partial pressure at AP initial concentration of 1.3 M is 11.1 % (see Figure 5.13), while at AP initial concentrations of 4 M and 5 M are 18.7 % and 11.7 %, respectively (see Figure 5.14).

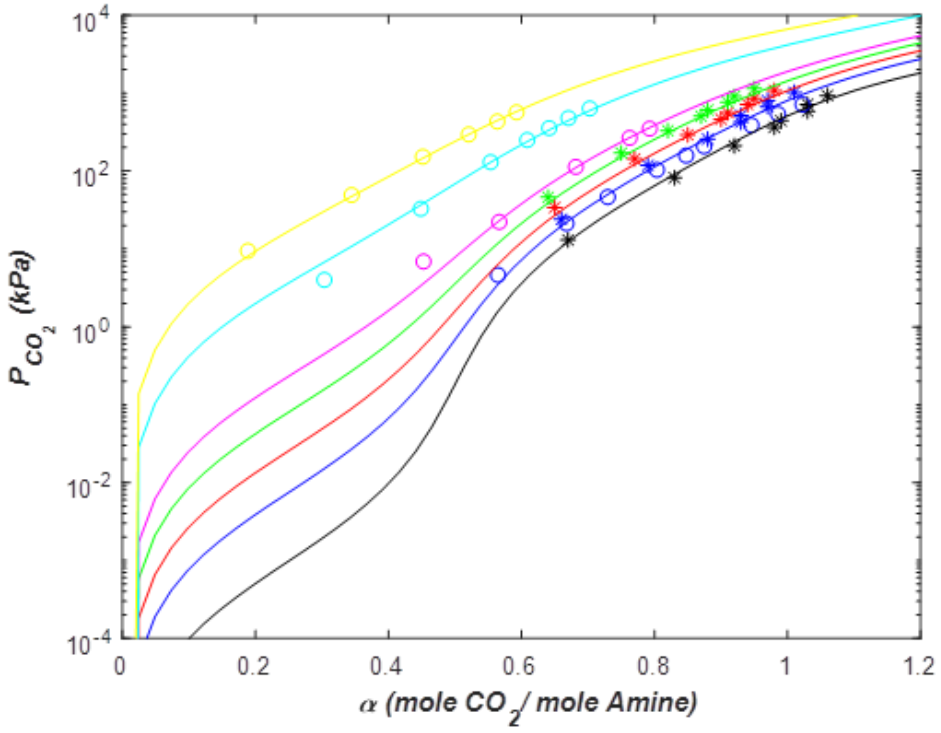

Figure 5.12 CO_2 partial pressure dependence as a function of loading at: 298 K (black color), 313 K (blue color), 323 K (red color), 333 K (green color), 343 K (pink color), 373 K (cyan color), 393 K (yellow color) and [AP] = 2 M, Solid lines - eNRTL model representation, * - Experimental data points [46]; o - Experimental data points [45];

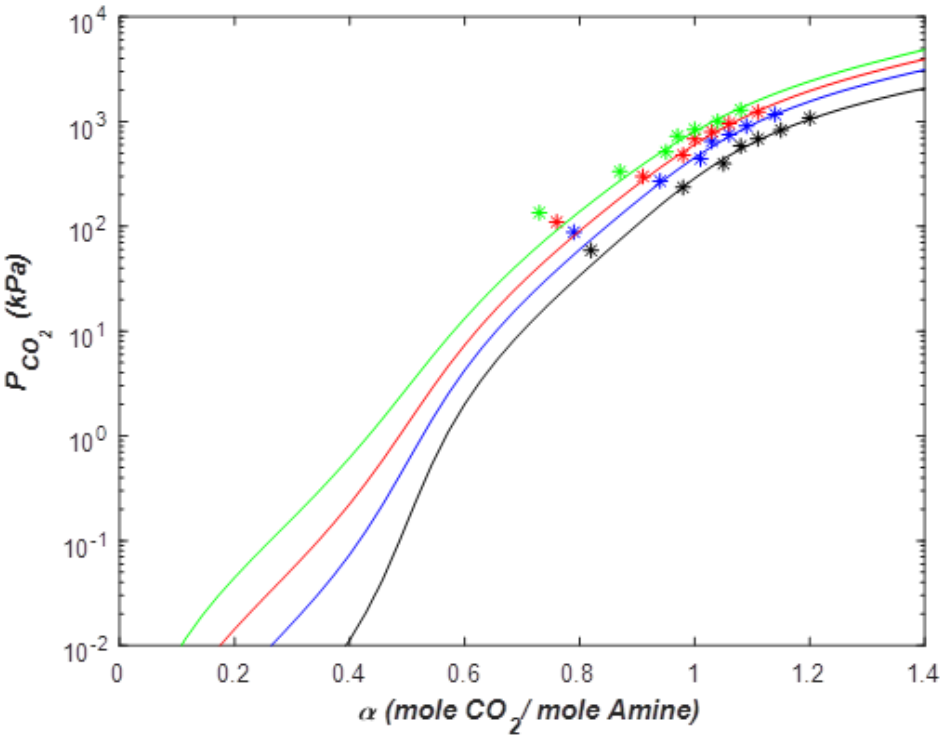

Figure 5.13 CO_2 partial pressure dependence as a function of loading at: 298 K (black color), 313 K (blue color), 323 K (red color), 333 K (green color) and [AP] = 1.3 M, Solid lines - eNRTL model representation,* - Experimental data points [46]

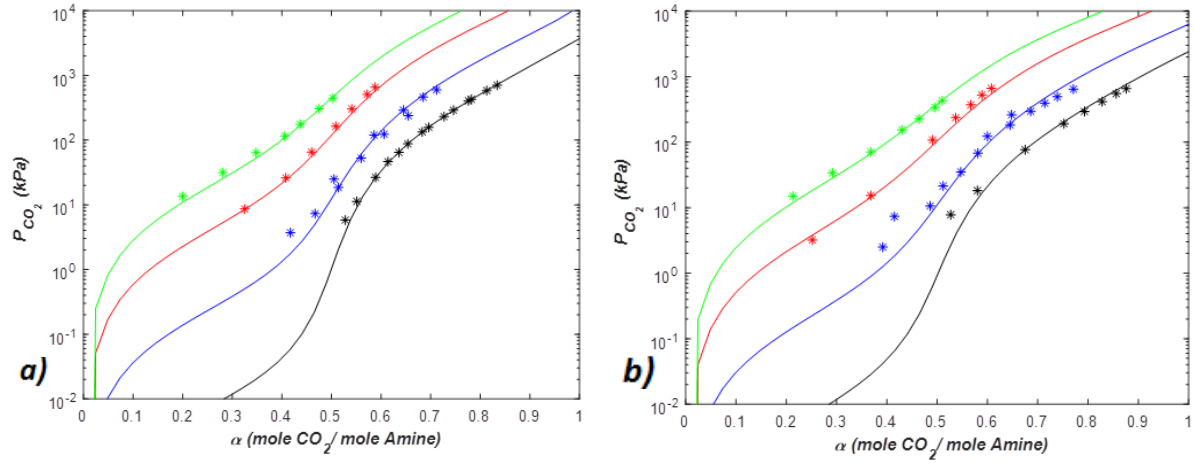

Figure 5.14 CO_2 partial pressure dependence as a function of loading at: 313 K (black color), 343 K (blue color), 373 K (red color), 393 K (green color); Solid lines - eNRTL model representation, * - Experimental data points [45]; a) [AP] = 5 M; b) [AP] = 4 M

5.2.1 Accuracy of the model

A total of 202 data points for CO_2 partial pressure were used in this work for the regression of the model parameters. Figure 5.15 shows a parity plot of the experimental versus model represented CO_2 partial pressure values. From the figure it can be seen that the data are in very good agreement with an average absolute relative deviation *AARD* of 16.3%, which is an acceptable deviation.

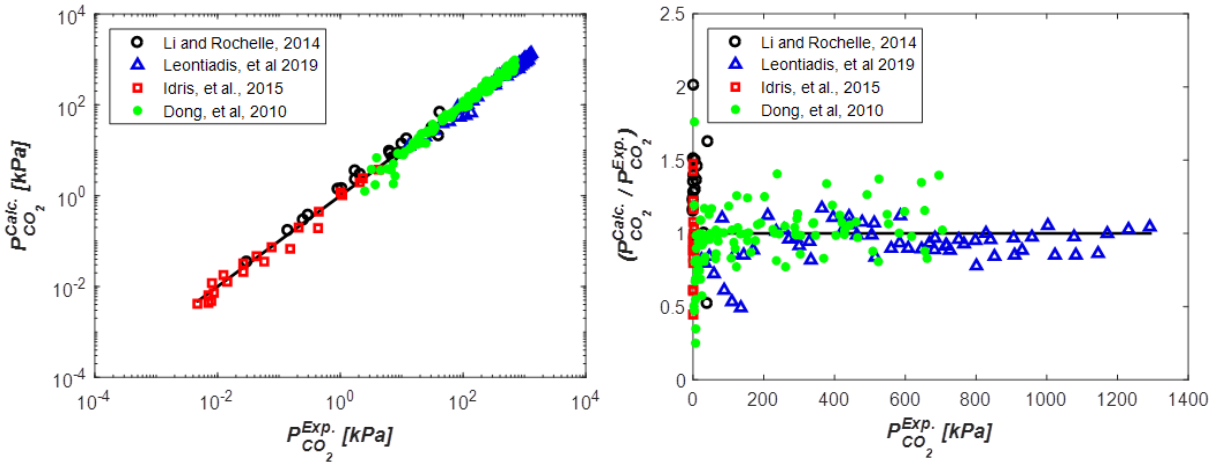

Figure 5.15 Parity plot between experimental and model represented CO_2 partial pressure

5.3 Speciation

An important consequence resulting from the rigorous thermodynamic modeling is the model ability to describe the concentration profiles of species in the liquid phase. Figure 5.16 shows the equilibrium concentration of the species of interest in 15 mass% AP aqueous solution ([AP] = 2 M) at 313 K and 333 K in the liquid phase. These temperatures were chosen as limits. Flue gas stream and the solvent are introduced into the absorption column at a temperature of about 313 K. The loaded AP solution leaving the bottom of the column has temperature of around 333 K. The model provides a reasonable description of the speciation. The green color represents the AP concentration which has a decreasing trend with the CO_2 loading due to the reaction with CO_2. The carbamate concentration reaches a maximum at CO2 loading of 0.5. On the other hand, CO_3^{2-} concentration is low up to the CO_2 loading of 0.4 and then is converted to HCO_3^-. The amount of protonated AP and HCO_3^- show an increasing trend with the CO_2 loading and are the main reaction products.

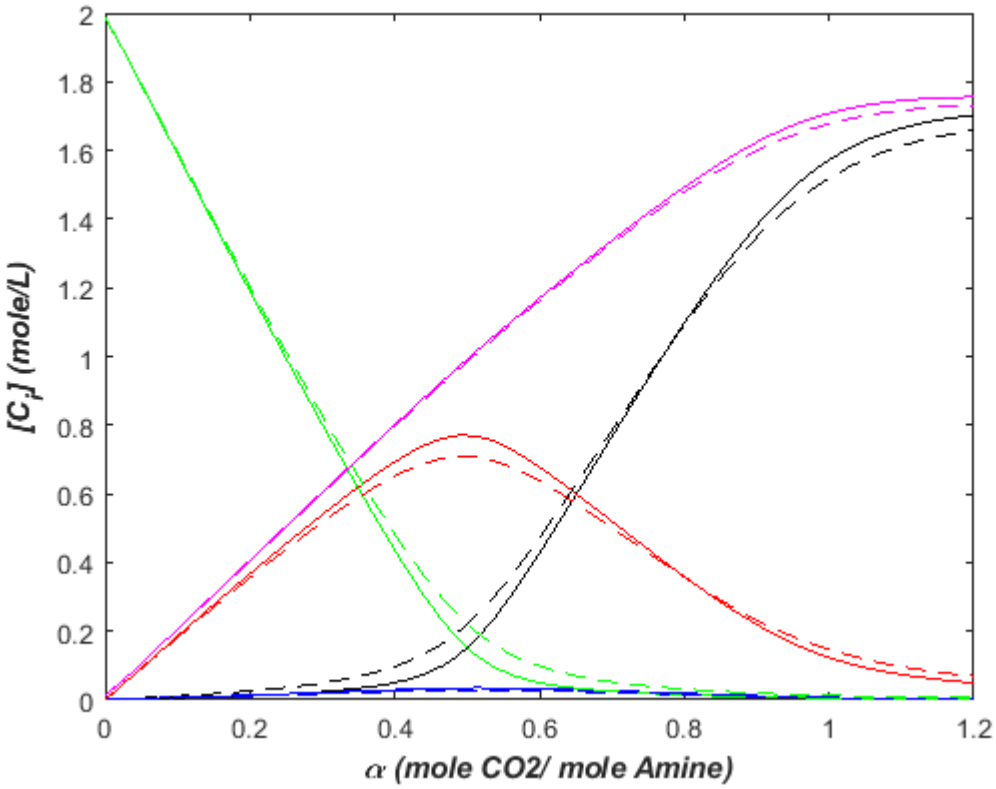

Figure 5.16 ***Model representation of the speciation in 15 mass % of AP ([AP] = 2 M) at: 313 K (Solid lines), 333 K (Dashed lines); Red color - $APCO_2^-$; Green color - AP; Pink color - APH^+; Black color - HCO_3^-; Blue color - CO_3^{2-}***

5.4 Heat of absorption

Another advantage of the rigorous modeling is its ability to describe the CO_2 absorption heat in aqueous AP solution. For these calculations, the optimization model was coupled with the model of Horton et al., which is based on the chemical equilibrium constants employing the Van't Hoff's approach (see equation 4.12). Figure 5.17 shows the model representation of heat contribution from each individual reaction occurring in the AP-H_2O-CO_2 system as a function of the CO_2 loading at 313 K. Unfortunately, no experimental data are available in the open literature to compare them with the calculated heat of absorption. For this reason, the heat of absorption was calculated for a commonly used primary alkanolamine, MEA, and the simulation results are shown in Figure 5.18. From the figures it can be seen that the model provided a common trend for CO_2 removal with alkanolamine solution. The contribution from carbamate formation is significant up to the CO_2 loading of 0.5, while at higher loadings bicarbonate formation predominates. Protonation reaction is the major contributor to the total heat of absorption up to the CO_2 loading of 1. Above this loading, as no unreacted AP remains in the system, the only dominant contribution is the physical dissolution of CO_2.

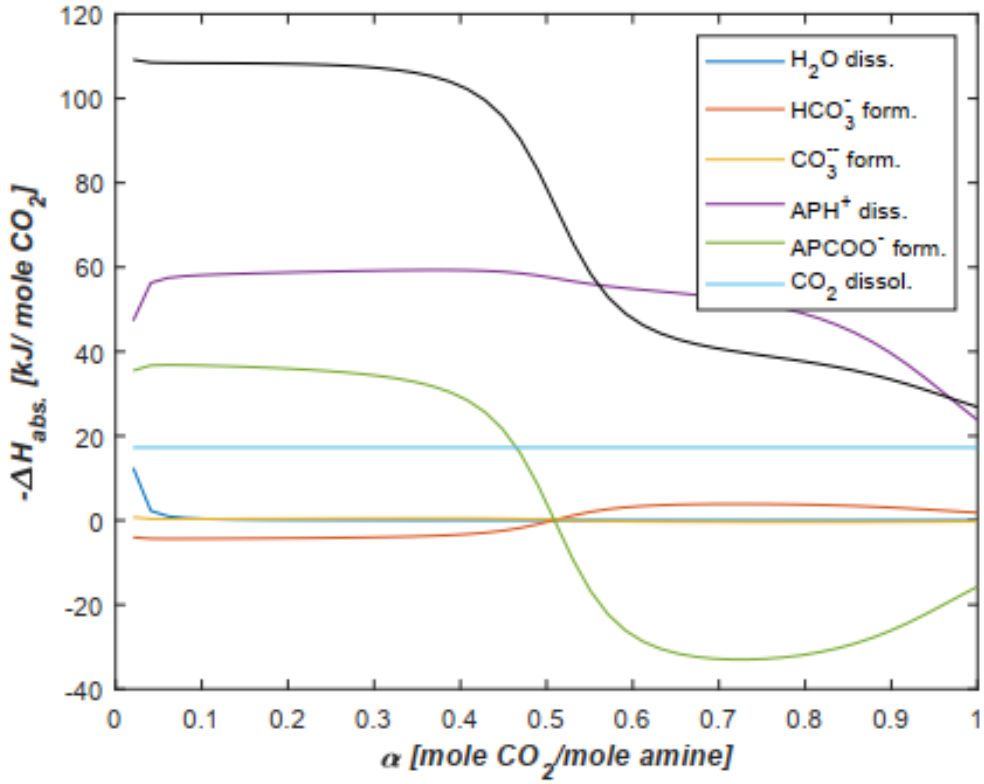

Figure 5.17 ***eNRTL model representation of the heat of absorption as a function of loading at 313 K and 15 mass % of AP ([AP] = 2 M); Black - total heat of absorption; Purple - heat of protonation of AP; Green - heat of carbamate formation; Cyan - heat of CO_2 dissolution; Red - heat of bicarbonate formation; Yellow - heat of carbonate formation; Blue - heat of water dissolution]***

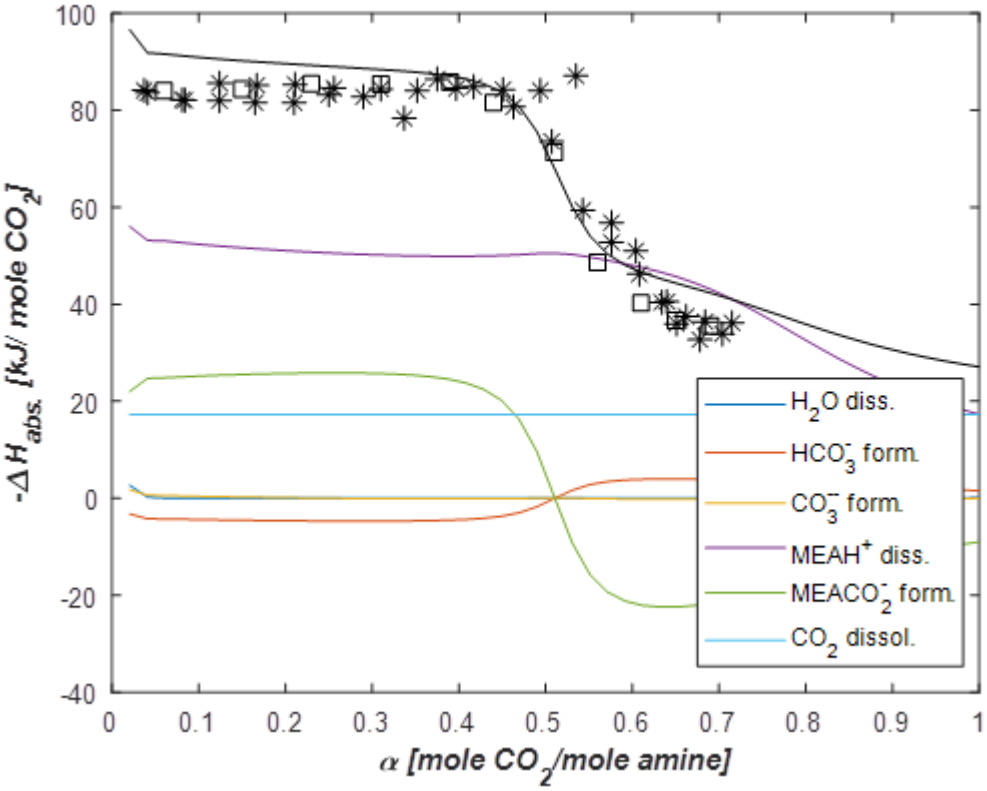

Figure 5.18 ***eNRTL model representation of the heat of absorption as a function of loading at 313 K and 30 mass % of MEA; Black - total heat of absorption; Purple - heat of protonation of AP; Green - heat of carbamate formation; Cyan - heat of CO_2 dissolution; Red - heat of bicarbonate formation; Yellow - heat of carbonate formation; Blue - heat of water dissolution; *, ▫ - Experimental data points [57]***

5.5 Discussion

In this work, two principal tasks were accomplished for the binary AP-water system and ternary AP-H_2O-CO_2 system. In the case of the binary system, four NRTL interaction parameters were selected to be regressed simultaneously using all available data. The model covers the entire range of AP concentrations and temperatures from 298 K to 373 K. In this way, we were able to construct a complete VLE dependences. The model prediction and experimental data are in excellent agreement resulting in *AARD* of 1.9 % for total pressure, *AARD* of 4.7 % for excess enthalpy and *AARD* of 0.5 % for the bubble point temperature data. Limitations of the NRTL model accuracy were found in the prediction of the excess heat capacity with the *AARD* of 56.7 % and these data were excluded from the fitting process.

Optimization of the ternary AP-H_2O-CO_2 system description was more challenging due to the large number of adjustable eNRTL parameters and a lack of experimental data. The model covers the range of AP concentrations in aqueous solution from 10 to 38 mass % (from 1.3 M to 7 M), temperatures from 298 K to 393 K and CO_2 loading from 0.2 to 1.2. However, most of the VLE data were reported at higher levels of CO_2 loading and there are no available data for the verification of the model prediction at lower CO_2 loadings. There was also a lack of data for the total pressure, physical CO_2 solubility and heat of absorption of CO_2 in the AP solution, which would be of a great help improving the developed model accuracy. The aim of this work was also to fill this lack of experimental data, but due to COVID 19 it was not possible to carry out measurements. The experimental and model representation of the CO_2 partial pressure values are in a good agreement with the *AARD* of 16.3 %.

6 Conclusion

In this work, an aqueous solution of 3-amino-1-propanol (AP) was investigated as a potential solvent for chemical removal of CO_2 from exhaust gases. A thermodynamic model representing the phase equilibrium of the binary AP-water system was developed in the MATLAB programming language using the NRTL model. The NRTL interaction parameters were regressed using the collected VLE data and excess enthalpy data from the literature. Thermodynamic consistency tests of the calculated VLE data were performed and the average absolute relative deviation between the model representation and the experimental data was calculated.

The calculated parameters together with the available VLE data were used in the regression of the interaction parameters for the ternary AP-H_2O-CO_2 system using the eNRTL framework. For the full representation of the ternary system, phase equilibrium was coupled with the chemical reactions in the liquid phase. The PSO optimization routine was developed in the MATLAB programming language and used in the regression analysis.

The model provides a very good description of the CO_2 partial pressure in the vapor phase, liquid phase speciation and a reasonable representation of the heat of absorption.

Regressed interaction parameters and chemical equilibrium constants in this work can be used in the design and simulation of the scrubbing technology.

Future work:

- Experimental estimation of the volatility of the solvent for estimation of the solvent losses and to design countermeasures to avoid solvent emissions in the process.

-Measurement of the vapor-liquid equilibrium of CO_2 in aqueous AP solution at lower CO_2 partial pressures at which there is a lack of experimental data.

- Experimental estimation of the physical solubility of CO_2 in aqueous AP solution (using the N_2O analogy) that can be used in the regression of the eNRTL parameters and to improve accuracy of the developed model.

- Measurement of the speciation in the liquid phase, heat of absorption of CO_2 in the liquid solvent as a function of temperature and CO_2 content for a better accuracy of the model representation.

References

[1] Rodé, E.D., Schaerer, L.A., Marinello, S. A., Hantelmann, G. V., Carbon Capture Storage Monitoring, ISBN 978-1-119-36348-4, 2018

[2] Rameshni, P. E., Flue Gas CO2 Capture with Aqueous Solvents; Monrovia, CA 91016, USA

[3] Commission of the European Communities. Communication from the Commission to the Council, the European parliament, the European Economic and Social Committee and the Committee of the Regions. Limiting Global Climate Change to 2 degree Celsius. The way ahead for 2020 andbeyond. Brussels, 10.1.2007. COM(2007) 2 final, EU: Brussels, Belgium

[4] Kapetaki, Z., Carbon Capture utilisation and storage, Publications Office of the European Union, ISBN 978-92-76-12440-5, 2019

[5] Pachauri, R. K., Meyer, L. A., Climate Change 2014: Synthesis Report, Intergovernmental Panel on Climate Change IPCC, ISBN 978-92-9169-143-2, 2015

[6] Olajire, A.A., CO2 capture and separation technologies for end-of-pipe applications – A review, Energy, 35, 2610-2628, 2010

[7] IEA (International Energy Agency), Energy Technology Perspectives 2017, OECD/IEA, Paris, 2017; https://www.iea.org/reports/energy-technology-perspectives-2017

[8] Feron, P. H.M., Hendriks, C. A., CO2 Capture Process Principles and Costs, Oil & Gas Science and Technology - Revue d'IFP Energies nouvelles, Institut Français du Pétrole, 60, 451-459, 2005

[9] Metz, B., Davidson, O., Coninck, H., Loos, M., Meyer, L., IPCC Special Report on Carbon Dioxide Capture and Storage, Intergovernmental Panel on Climate Change, ISBN-13 978-0-521-86643-9, 2005

[10] Asif, M., Suleman, M., Haq, I., Post-combustion CO 2 capture with chemical absorption and hybrid system: current status and challenges: Review: Hybrid systems for post-combustion CO 2 capture, Greenhouse Gases: Science and Technology, 34, 2018

[11] Rochelle, G. T., Amine Scrubbing for CO Capture, International Journal of Clean Coal and Energy, 325, 1652-1654, 2009

[12] Jens, C. M., Modeling and Characterization of Liquid Vapor Equilibrium of N-methyl-1,3-Propanediamine for CO2 Capture, Norwegian University of Science and Technology, 2011

[13] Bernhardsen, I. M., Trollebø, A. A., Perinu, C., Knuutila, H., Vapour-liquid equilibrium study of tertiary amines, single and in blend with 3-(methylamino)propylamine, for post-combustion CO2 capture, Journal of Chemical Thermodynamics, 138, 211-228, 2019

[14] Liang, Z., Rongwong, W., Liu, H., Fu, K., Gao, H., Cao, F., Zhang, R., Sema, T., Henni, A., Sumon, K., Nath, D., Gelowitz, D., Srisang, W., Saiwan, C., Benamor, A., Al-

Marri, M., Shi, H., Supap, T., Chan, C., Zhou, Q., Abu-Zahra, M., Wilson, M., Olson, W., Idem, R., Tontiwachwuthikul, P., Recent progress and new developments in post-combustion carbon-capture technology with amine based solvents, International journal of greenhouse gas control, 40, 26-54, 2015

[15] Kohl, A. L., Nielsen, R. B., Gas Purification (fifth edition), Elsevier, ISBN 978-0-88415-220-0, 1997,

[16] McMurry, J. E., Organic Chemistry (3rd ed.), Belmont: Wadsworth, ISBN 0-534-16218-5, 1992

[17] Bernhardsen, I. M., Knuutila, H. K., A review of potential amine solvents for CO2 absorption process: Absorption capacity, cyclic capacity and pKa, International journal of greenhouse gas control, Ullmann's Encyclopedia of Industrial Chemistry, 61, 27-48, 2017

[18] Frauenkron, M., Mmelder, J. P., Ruider, G., Rossbacher, T., Hoke, H., Ethanolamines and Propanolamines, 13, 405-428, 2012

[19] Dong, L., Chen, J., Gao, G., Solubility of Carbon Dioxide in Aqueous Solutions of 3-Amino-1-propanol, Journal of Chemical & Engineering Data, 55, 1030-1034, 2010

[20] Singh, P., Niederer, J., Versteeg, G., Structure and activity relationships for amine based CO2 absorbents, International journal of greenhouse gas control, 1, 5-10, 2007

[21] Mundhwa, M., Calorimetric measurements of the molar heat capacity and the molar excess enthalpy for various alkanolamines in aqueous solutions, Master's Thesis, ISBN: 978-0-494-29156-6, 2007

[22] Kohl, L.A., Nielsen, B.R., Gas Purification, Gulf Professional Publishing, ISBN: 9780080507200, 1997

[23] Elliot, J. R., Lira, C. T., Introductory chemical engineering thermodynamics, Prentice-Hall, ISBN-13: 9780136068549, 1999

[24] Prausnitz, J. M., Lichtenthaler, R. N., Gomes de Azevedo, E., Molecular Thermodynamics of FluidPhase Equilibria, Prentice-Hall, ISBN: 0-13-977745-8, 1999

[25] Michelsen, M. L., Mollerup, J. M., Thermodynamic models: Fundamentals and computational aspects, Tie-Line Publications, ISBN: 87-989961-3-4, 2007

[26] Vetere, A., Prediction of vapour-liquid equilibria of non-aqueous systems in the subcritical range by using the NRTL equation, Fluid Phase Equilibria, 91, 265-280, 1993

[27] Renon, H., Prausnitz, J.M., Local compositions in thermodynamic excess functions for liquid mixtures, American Institute of Chemical Engineers Journal, 14, 135–144, 1968

[28] Graczová, E., Steltenpohl, P., Application of extended NRTL equation for ternary liquid-liquid and vapour-liquid-liquid equilibria description, Chemical Papers- Slovak Academy of Sciences, 64, 310-317, 2010

[29] Schmidt, K. A. G., Maham, Y., Mather, A. E., Use of the NRTL equation for simultaneous correlation of vapor-liquid equilibria and excess enthalpy, Journal of Thermal Analysis and Calorimetry, 89, 61-72, 2007

[30] Demirel, Y., Calculation of Excess Entropy for Binary Liquid Mixtures by the NRTL and UNIQUAC Models, The Journal of Chemical Thermodynamics, 33, 2875-2878, 1994

[31] Chen, C. C., A Local Composition Model for the Excess Gibbs Energy of Electrolyte Systems I: Single Completely Dissociated Electrolyte, Single-Solvent Systems, American Institute of Chemical Engineers Journal, 28, 588, 1982

[32] Chen, C. C., Evans, I. B., A Local Composition Model for the Excess Gibbs Energy of Aqueous Electrolyte Systems, American Institute of Chemical Engineers Journal, 32, 444-454, 1986

[33] Hessen, E. T., Haug-Warberg, T., Svendsen, H. F., The refined e-NRTL model applied to CO2-H2O-alanolamine systems, Chemical Engineering Science, 65, 3638-3648, 2010

[34] Wisniak, J., The Herington Test for Thermodynamic Consistency, Industrial & Engineering Chemistry Research, 33, 177-180, 1994

[35] Kurihara, K., Egawa, Y., Ochi, K., Kojima, K., Evaluation of thermodynamic consistency of isobaric and isothermal binary vapor–liquid equilibrium data using the PAI test, Fluid Phase Equilibria, 219, 75-85, 2004

[36] Li, H., Frailie, P.T., Rochelle, G.T., Chen, J., Thermodynamic modeling of piperazine/2-aminomethylpropanol/CO2/water, Chemical Engineering Science, 117, 331-341, 2014

[37] DECHEMA Deutsche Gesellschaft fur Chemisches Apparatewesen, Chemische Technik und Biotechnologie e. V. Postfach 15 01 04, D-60061 Frankfurt am Main, Germany, 2003, ISBN: 3-89746-053-X

[38] Mundhwa, M., Henni, A., Calorimetric measurements of the molar heat capacity and the molar excess enthalpy for various alkanolamines in aqueous solutions, Journal of Chemical & Engineering Data, 52, 491-498, 2007

[39] Hessen, E.T., Haug-Warberg, T., Svendsen, H.F., The refined e-NRTL model applied to CO2-H2O-alkanolamine systems, Chemical Engineering Science, 65, 3638-3648, 2010

[40] Austgen, D.M., Rochelle, G.T., Peng, X., Chen, C.C., Model of vapor-liquid equilibria for aqueous acid gas-alkanolamine systems using the electrolyte-NRTL equation, Industrial & Engineering Chemistry Research, 28, 1060-1073, 1989

[41] Moosavi, S.R., Wood, D.A., Samadani, S.A., Modeling Performance of Foam-CO2 Reservoir Flooding with Hybrid Machine- learning Models Combining a Radial Basis Function and Evolutionary Algorithms, Computational Research Progress in Applied Science & Engineering, 06, 1-8, 2020

[42] Zhang, K., Hawrylak, B., Palepu, R., Tremaine, P.R., Thermodynamics of aqueous amines: excess molar heat capacities, volumes, and expansibilities of {water+ methyldiethanolamine (MDEA)} and {water + 2-amino-2-methyl-1-propanol (AMP)}, Journal of Chemical & Engineering Data, 34, 679-710, 2002

[43] Idris, Z., Peresunko, N., Jens, K.J., Eimer, D.A., Equilibrium solubility of carbon dioxide in aqueous solutions of 3-amino-1-propanol, 4-amino-1-butanol and 5-amino-1-pentanol at low partial pressures, Fluid Phase Equilibria, 387, 81- 87, 2015

[44] Le Li, Rochelle, G.T., CO2 mass transfer and solubility in aqueous primary and secondary amine, Energy Procedia, 63, 1487-1496, 2014

[45] Dong, L., Chen, J., Gao, G., Solubility of Carbon Dioxide in Aqueous Solutions of 3-Amino-1-propanol, Journal of Chemical & Engineering Data, 55, 1030-1034, 2020

[46] Leontiadis, K., Tzimpilis, E., Aslanidou, D., Tsivintzelis, I., Solubility of CO2 in 3-amino-1-propanol and in N-methyldiethanolamine aqueous solutions: Experimental investigation and correlation using the CPA equation of state, Fluid Phase Equilibria, 2019

[47] Aspen Technology Inc., Aspen Physical Property System, V-7.1, 2008, Cambridge

[48] Dash, S.K., Samanta, A.N., Bandyopadhyay, S. S., (Vapour + liquid) equilibria (VLE) of CO2 in aqueous solutions of 2-amino-2-methyl-1-propanol: New data and modelling using eNRTL-equation, The Journal of Chemical Thermodynamics, 43, 1278-1285, 2011

[49] Schwabe, K., Graichen, W., Spiethoff, D., Physicochemical investigations on alkanolamines, Zeit. Physik. Chemie (Munich), 20, 68–82, 1959

[50] Posey, M.L., Rochelle, G.T., A Thermodynamic Model Methyldiethanolamine − CO2 −H2S−Water, Industrial & Engineering Chemistry Research, 36, 3944–395, 1997

[51] Kennedy, J., Eberhart, R., Particle Swarm Optimization, Proceedings of ICNN'95 - International Conference on Neural Networks, 1942-1948, 1995

[52] Clerc, M., Kennedy, J., The particle swarm - explosion, stability, and convergence in a multidimensional complex space, IEEE Transactions on Evolutionary Computation, 6, 58–73, 2002

[53] Luo, Y., Xigang, Y., Yongjian, L., An improved PSO algorithm for solving non-convex NLP/MINLP problems with equality constraints, Computers & Chemical Engineering, 31, 153 – 162, 2007

[54] L. Zheng (2015): Thermodynamic Modelling of Liquid–liquid Equilibria Using the Nonrandom Two-Liquid Model and Its Applications

[55] Austgen, D. M., Rochelle, G. T., Peng, X., Chen, C. C., Model of vaporliquid equilibria for aqueous acid gas-alkanolamine systems using the electrolyteNRTL equation, Industrial & Engineering Chemistry Research, 28, 1060–1073, 1989

[56] Bishnoi, S., Rochelle, G. T., Thermodynamics of piperazine/ methyldiethanolamine/ water/carbon dioxide, Industrial & Engineering Chemistry Research, 41, 604–612, 2002

[57] Kim, I., Hoff, K. A., Hessen, E. T., Haug-Warberg, T., Svendsen, H. F., Enthalpy of absorption of CO2 with alkanolamine solutions predicted from reaction equilibrium constants, Chemical Engineering Science, 64, 2027-2038, 2009

Appendix 1

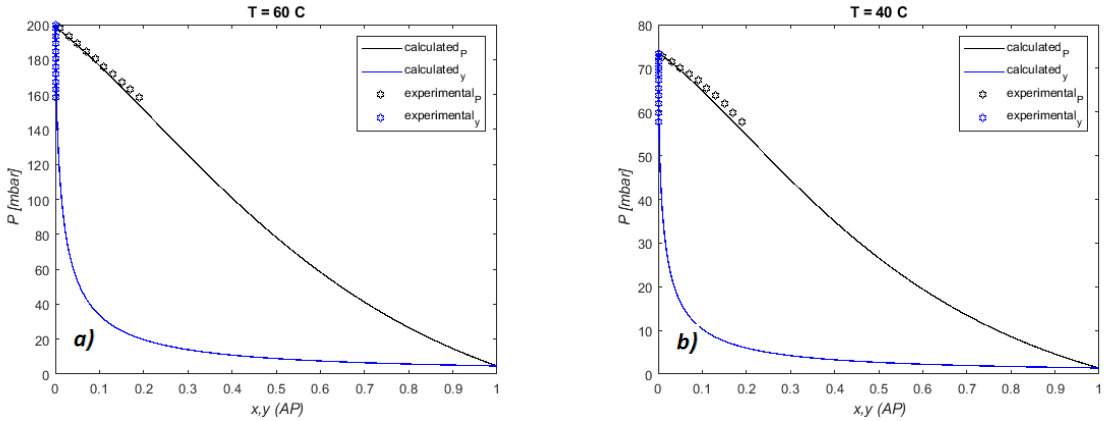

Figure A1: Isothermal Pxy diagram for binary AP - water system at: a) 333 K, b) 313 K (Points from in-house VLE data), Black solid lines – calculated boiling curves; Blue solid lines – calculated dew point curves; *- Experimental data points

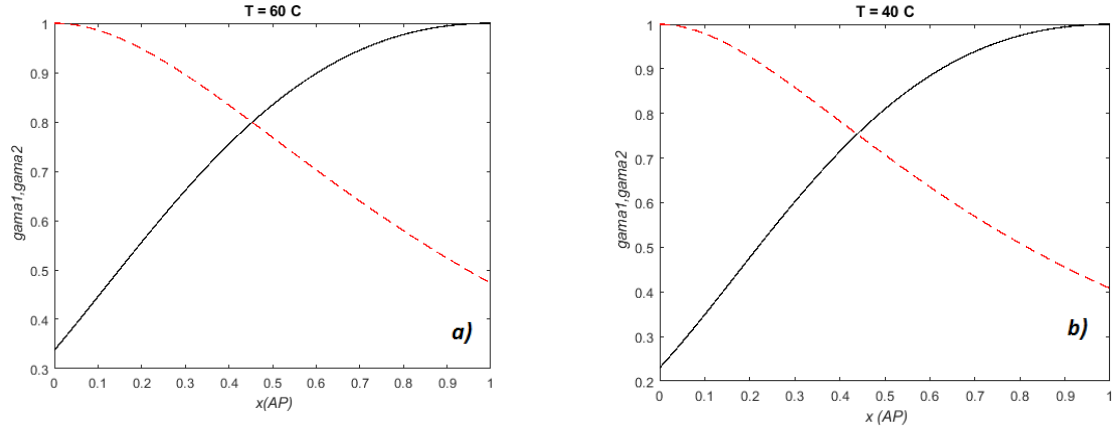

Figure A2: Activity coefficients of AP at: a) 333 K, b) 313 K, (Points from in-house VLE data); Black solid lines - γ_{AP}; Red dotted lines - γ_{Water}

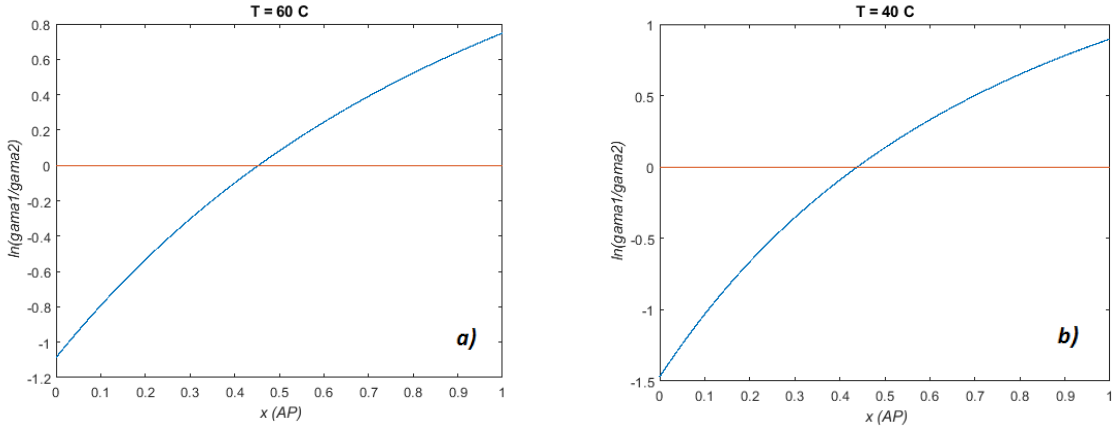

Figure A3: Test of thermodynamic consistency for binary AP-water system at: a) 333 K, b) 313 K (Points from in-house VLE data);

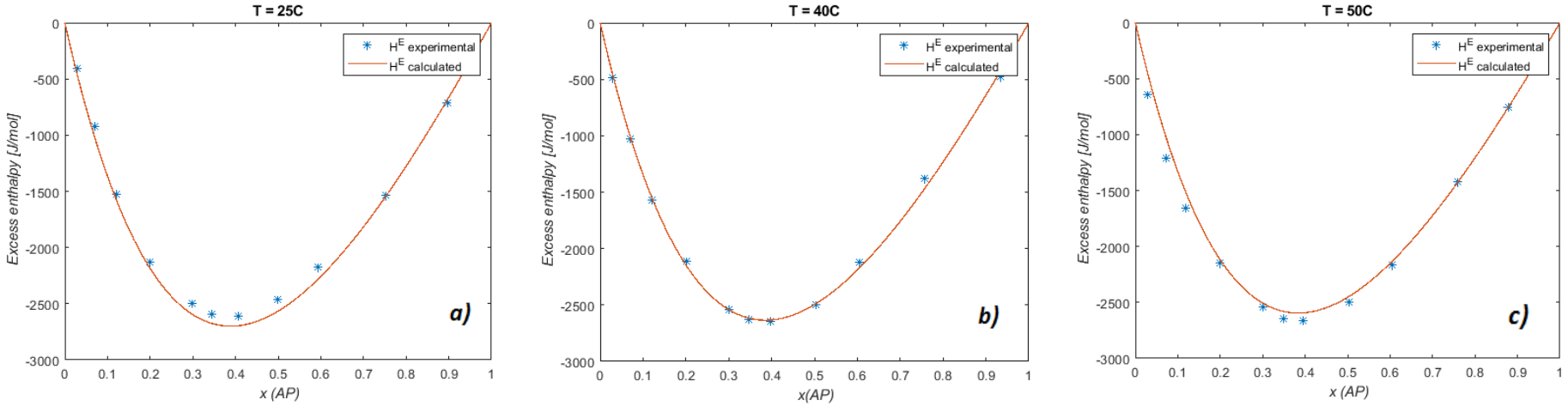

Figure A4: Excess enthalpy dependence of the AP-water mixture composition at: a) 298 K (black color), b) 313 K (blue color), c) 323 K (red color); Solid lines – NRTL model, *–Experimental data points [38]

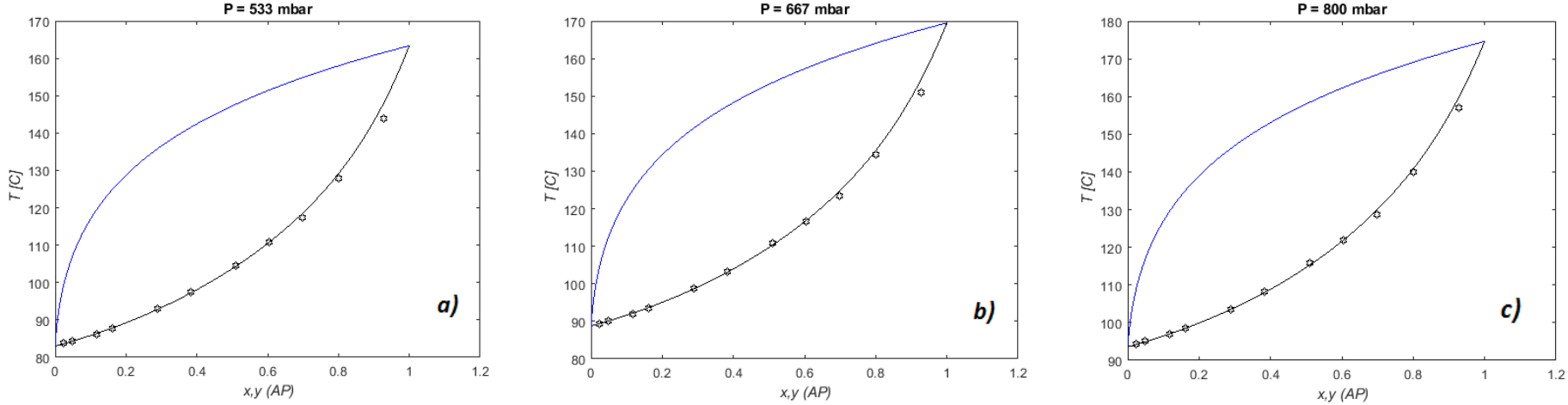

Figure A5: Isobaric Txy data for binary AP-water system at: a) 533 mbar (blue color), b) 667 mbar (red color), c) 800 mbar (green color); Solid lines – NRTL model; *–Experimental data points [37]

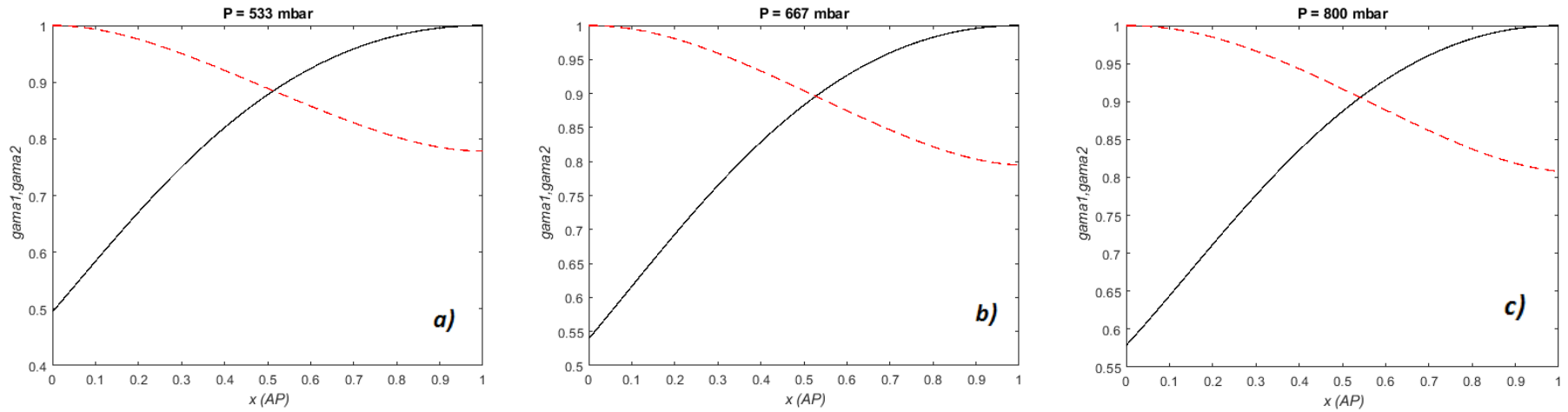

Figure A6: Activity coefficients of AP at: a) 533 mbar, b) 667 mbar, c) 800 mbar (Points [37]); Black solid lines - γ_{AP}; Red dotted lines - γ_{Water}

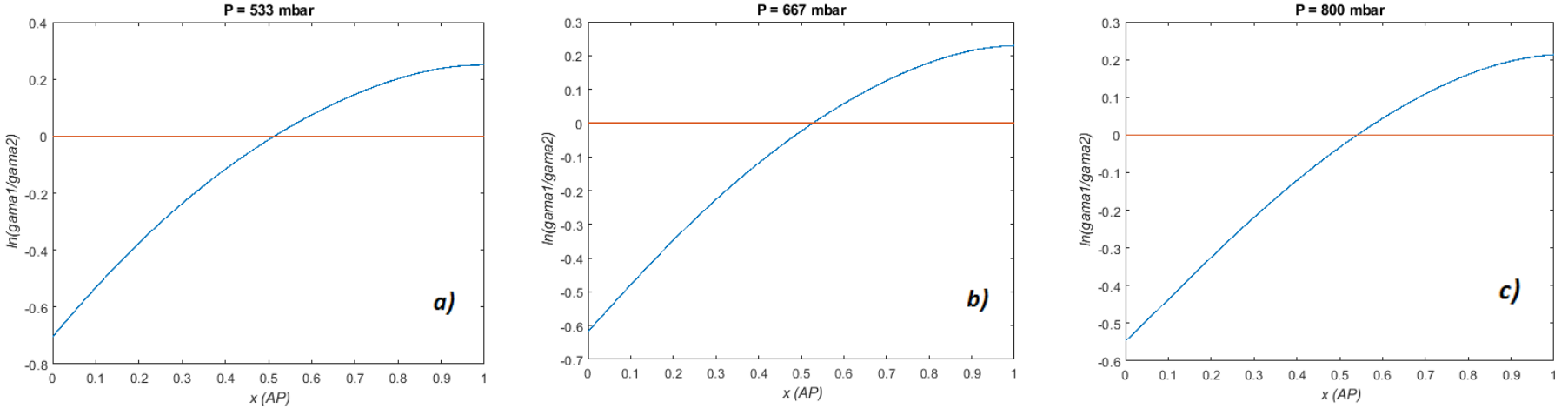

Figure A7: Test of thermodynamic consistency for binary AP-water system at: a) 533 mbar, b) 667 mbar, c) 800 mbar (Points [37]);

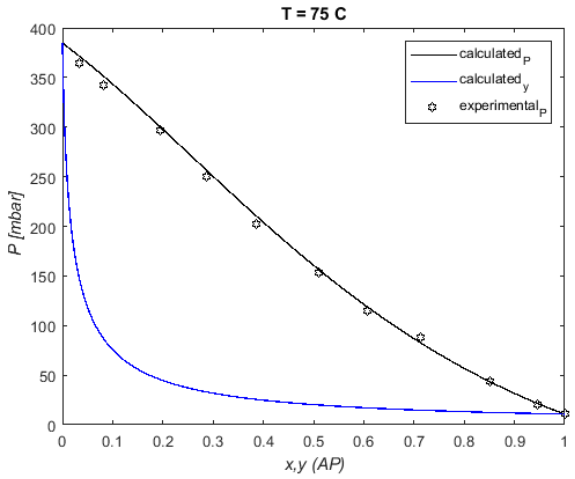

Figure A8: Isothermal Pxy diagram for binary AP - water system at: 348 K (Points [37]). Black solid lines – calculated boiling curves; Blue solid lines – calculated dew point curves; *- Experimental data points;

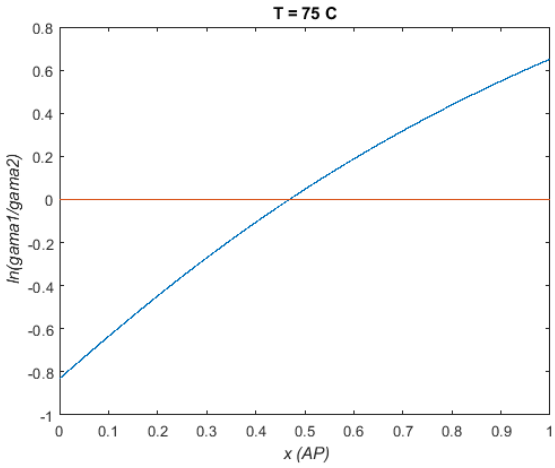

Figure A9: Test of thermodynamic consistency for binary AP-water system at: 348 K (Points [37]);

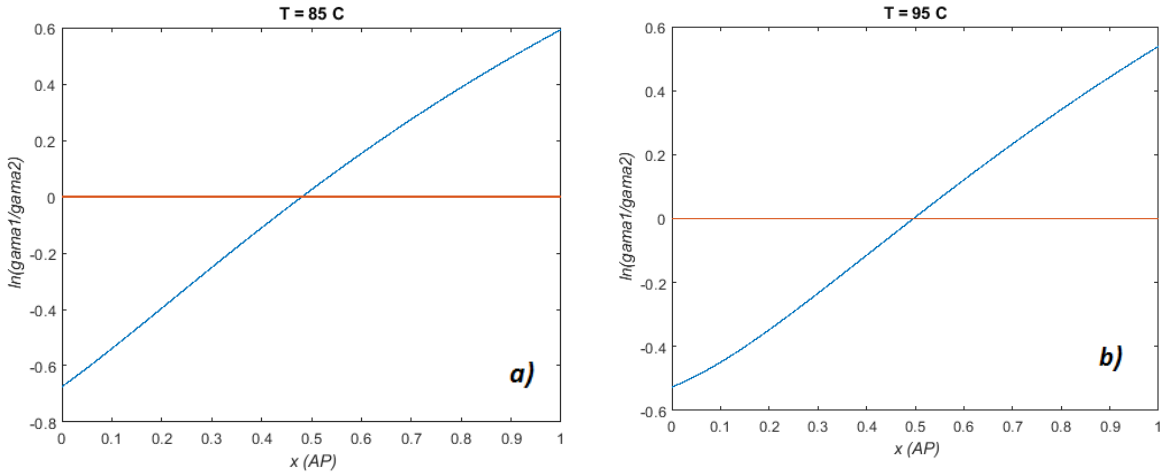

Figure A10: Test of thermodynamic consistency for binary AP-water system at: a) 358 K, b) 368 K, (Points [37]);

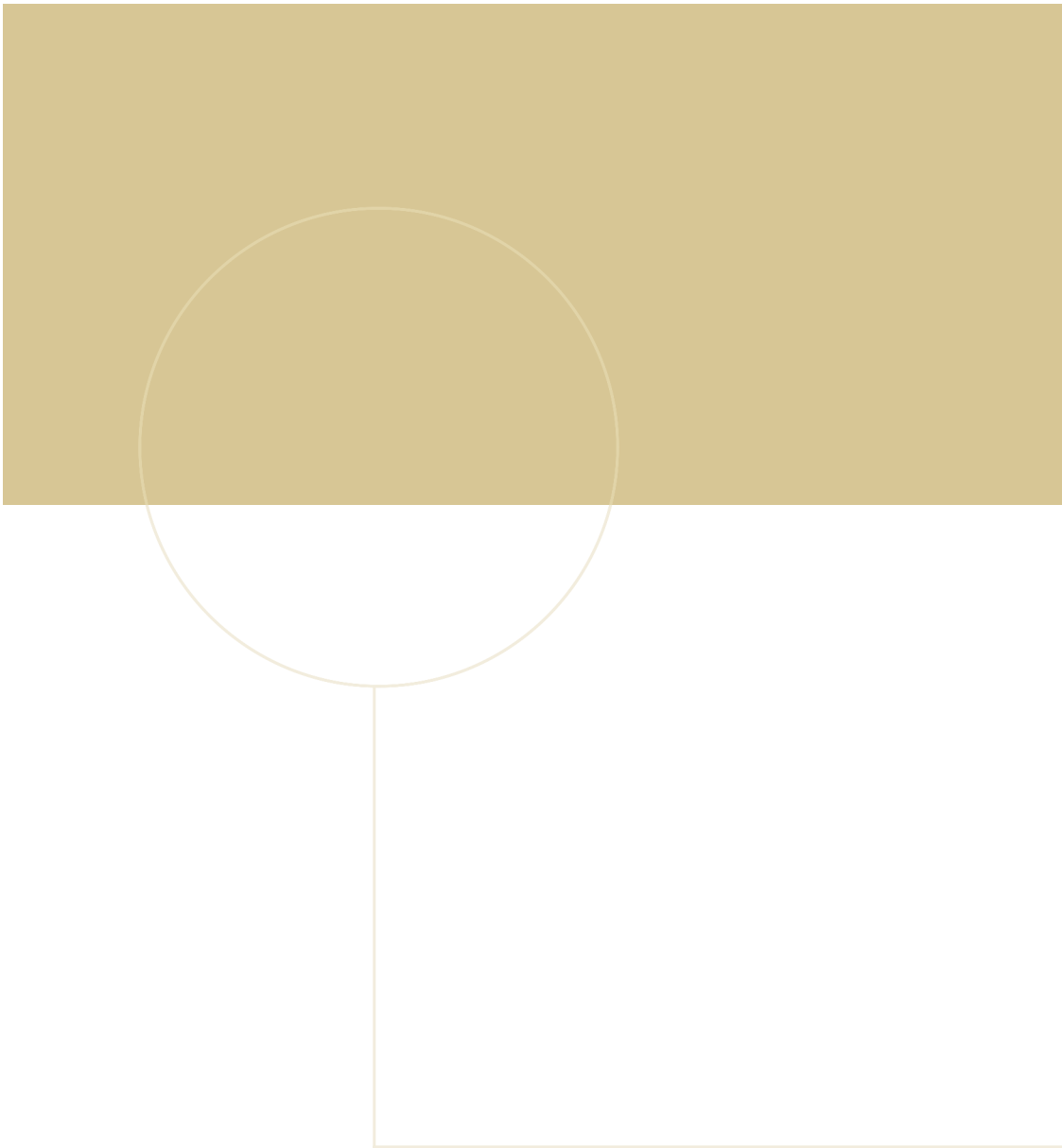

NTNU

Norwegian University of
Science and Technology